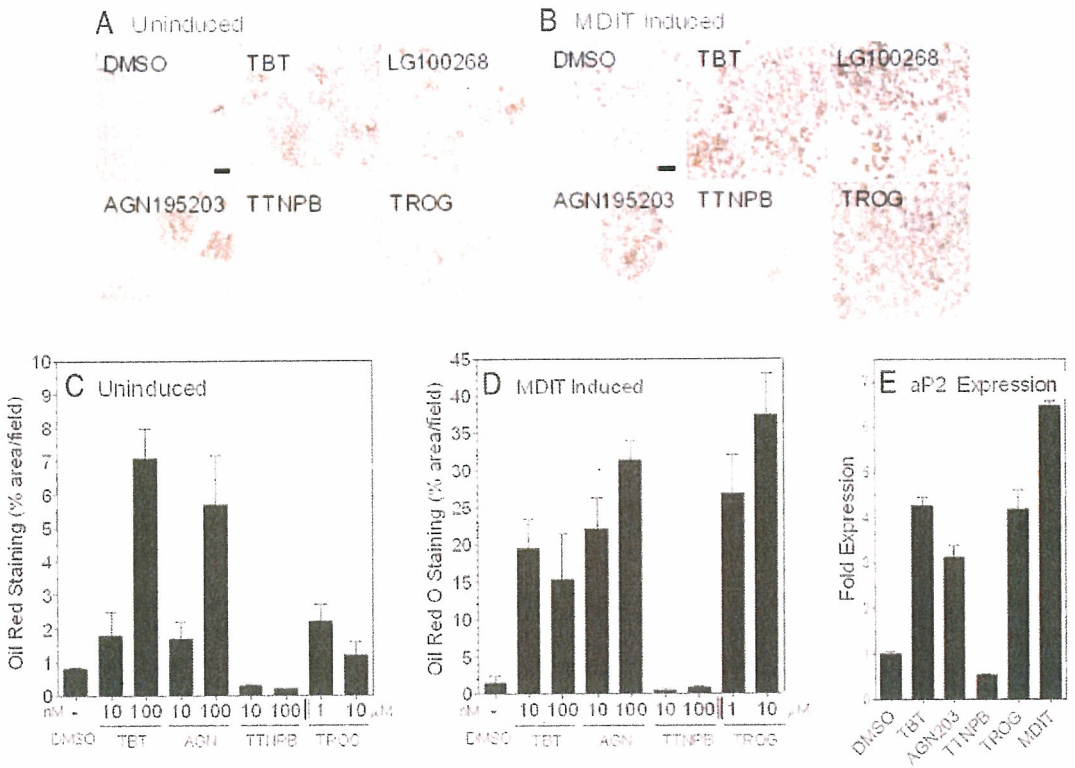

Fig. 2. Tributyltin Induces Adipogenesis in 3T3-L1 Cells

Uninduced (A) and MDIT-induced (B) 3T3-L1 cultures grown for 1 wk in the presence of vehicle (DMSO), or ligands were analyzed for mature adipocyte differentiation by Oil Red O staining. *Scale bar* represents 100 μm. C and D, The percentage area stained was determined by automated analysis of random fields (n = 9) from high-contrast dissecting scope photographs of monolayers analyzed in ImageJ; 1–100 nM of TBT, AGN195203, and TTNPB or 1–10 μM troglitazone. E, Quantitative real-time PCR (QRT-PCR) of adipocyte-specific fatty acid binding protein aP2 (aP2/Fabp4) expression levels in postconfluent 3T3-L1 cells treated with the indicated ligands for 24 h. Data were normalized to glyceraldehyde-3-phosphate dehydrogenase controls and plotted as average fold induction ± SEM (n = 3).TROG, Troglitazone.

yielded a K_i of 300 nM, consistent with its published K_d (28). The K_d values for TBT binding to RXRα (12.5 nM) and PPARγ (20 nM) are also in close agreement with EC_{50} values obtained from transient transfection assays using GAL4-RXRα and GAL4-PPARγ constructs (Table 2).

Taken together, these data show that organotins such as TBT, although structurally distinct from previously described natural or synthetic ligands, can interact with RXRα and PPARγ, via direct ligand binding to induce productive receptor-coactivator interactions and promote transcription in a concentration-dependent manner. Organotins are therefore potent nanomolar receptor activators on par with synthetic RXR and PPARγ ligands such as LG100268, AGN195203, and thiazolidinediones.

TBT Promotes Adipogenesis in the Murine 3T3-L1 Cell (Embryonic Murine Preadipocyte Fibroblast Cell Line) Model

Numerous studies have demonstrated the critical role played by RXRα:PPARγ signaling in regulation of mammalian adipogenesis (29–31). In the murine 3T3-L1 preadipocyte cell model, adipogenic signals induce early key transcriptional regulators such as CCAAT/enhancer binding proteins (C/EBPs) β and δ that lead to mitotic clonal expansion of growth-arrested preadipocytes and induction of the late differentiation factors C/EBPα and PPARγ (32–34). The combination of C/EBPα expression together with PPARγ signaling efficiently drives terminal adipocyte differentiation and lipid accumulation. We therefore tested whether TBT signaling through RXR:PPARγ could promote adipogenesis in the murine 3T3-L1 differentiation assay and compared its effect to other RXR-specific or PPARγ ligands (Fig. 2). Undifferentiated 3T3-L1 cells were cultured for 1 wk in the presence of ligands either with or without a prior 2-d treatment with MDIT (an adipogenic-sensitizing cocktail of 3-isobutyl-1-methylxanthine, dexamethasone, insulin, and T_3) (35). Cells were then scored for lipid accumulation using Oil Red O staining to determine the degree of terminal adipocyte differentiation. TBT was as effective as LG100268 or AGN195203 in promoting dif-

ferentiation in the absence of MDIT treatment, increasing the number of differentiated adipocytes about 7-fold over solvent-only controls (Fig. 2, A and C). The PPARγ agonist troglitazone was a weak inducer in the absence of MDIT. Prior treatment with MDIT increased the response to TBT, LG100268, and AGN195203 a further 3- to 5-fold (Fig. 2, B and D). MDIT treatment also boosted the response to troglitazone to equivalent levels as expected from published studies showing that combination treatment with PPARγ ligands promotes efficient adipocyte differentiation (36–38). In contrast, the RAR agonist TTNPB inhibited the differentiation of 3T3-L1 cells, consistent with previously published data that showed RAR signaling blocks adipogenesis during the early stages of differentiation *in vitro* and can modulate adiposity and whole body weight *in vivo* (39–41). The differential response of 3T3-L1 cells to receptor-selective retinoids indicates that TBT favors RXR homodimer or permissive RXR-heterodimer rather than RXR:RAR signaling in this cell model.

Adipocyte differentiation by TBT was accompanied by direct transcriptional effects on RXR:PPARγ targets such as adipocyte-specific fatty acid-binding protein (aP2) mRNA. The aP2 promoter contains response elements sensitive to C/EBP factors and RXRα:PPARγ signaling (42). Quantitative real-time PCR analysis showed aP2 levels were elevated by TBT treatment approximately 5-fold at 24 h (Fig. 2E) and 45-fold at 72 h (data not shown). LG100268, troglitazone, and MDIT treatment also increased aP2 expression at these time points whereas the RAR agonist TTNPB was inhibitory, consistent with the observed cellular responses.

TBT Induces Adipogenic Regulators and Markers of RXRα:PPARγ Signaling *in Vivo*

The ability of organotins to regulate RXRα:PPARγ target genes and key modulators of adipogenesis and lipid homeostasis *in vivo* has not been previously examined. Therefore, we next asked whether TBT could perturb expression of critical transcriptional mediators of adipogenesis such as RXRα, PPARγ, C/EBPα/β/δ, and sterol regulatory element binding factor 1 (Srebf1) as well as known target genes of RXRα:PPARγ signaling from liver, epididymal adipose tissue, and testis of 6-wk-old male mice dosed for 24 h with TBT [0.3 mg/kg body weight (b.w.)], AGN195203 (0.3 mg/kg b.w.), troglitazone (3 mg/kg b.w), or vehicle (corn oil) administered by ip injection. TBT either had no effect or weakly repressed RXRα and PPARγ transcription in liver (Fig. 3, A and B). A more pronounced decrease was observed for RXRα, PPARγ, C/EBPα, and C/EBPδ in adipose tissue and testis (Fig. 3, B and C). In contrast, TBT, AGN195203, and troglitazone significantly induced expression of the early adipogenic transcription factor C/EBPβ in liver and testis, whereas it was more weakly induced in adipose tissue. Induction was strongest in testis where TBT and troglitazone increased expression greater than 10-fold and AGN195203 increased expression 60-fold compared with vehicle controls (Fig. 3C). In addition to C/EBPβ, the proadipogenic transcription factor Srebf1 was also significantly increased in adipose tissue by all three receptor ligands and weakly induced in liver.

We also observed coordinate changes in several well-characterized direct target genes of RXR:PPARγ signaling. Fatty acid transport protein (Fatp) acts as a key control point for regulation of cellular fatty acid content. The Fatp promoter contains a functional PPAR response element shown to be sensitive to RXR:PPARγ signaling in 3T3-L1 adipocytes and white fat (43–46). Fatp mRNA levels were up regulated 2- to 3-fold in liver and epididymal adipose tissue but not testis by TBT, AGN195203, and troglitazone (see Fig. 5, A and B). Similarly, the PPARγ target phosphoenolpyruvate carboxykinase 1 (PEPCK/Pck1) (47), the rate-limiting step in hepatic gluconeogenesis and adipose glyceroneogenesis, was up-regulated in liver and adipose tissues by TBT or troglitazone treatment.

Signaling through RXR:PPARγ, RXR:LXR, and ADD1/Srebf1 in hepatocytes has been shown to modulate fatty acid synthesis through transcriptional control of acetyl-coenzyme A carboxylase (Acac), the rate-limiting step in long-chain fatty acid synthesis (48, 49), as well as fatty acid synthase (Fasn) (50–53). Hepatic expression of both Acac and Fasn was unregulated between 1.5–2.5-fold by TBT, AGN195203, and troglitazone. Therefore, the coordinate increased expression of Fatp, Pck1, Acac, and Fasn in liver suggests that TBT stimulates fatty acid uptake and triglyceride synthesis. Similar changes have been reported in the induction of hepatic steatosis by overactive PPARγ signaling (49, 54).

Taken together, these data show that TBT exposure induces lipogenic RXR:PPARγ target gene expression, in adipose tissue and liver, and modulates associated early adipocyte differentiation factors such as C/EBPβ and Srebf1. We inferred from these data that organotins are potential adipogenic agents *in vivo*.

Developmental Exposure to TBT Disrupts Lipid Homeostasis and Adipogenesis in Vertebrates

Based on its molecular pharmacology, ability to induce 3T3-L1 adipocyte differentiation, and *in vivo* transcriptional responses, we reasoned that TBT would disrupt normal endocrine control over lipid homeostasis and impact adipogenesis, particularly when exposure occurred during sensitive periods of development. We therefore tested this hypothesis in two vertebrate model systems, mouse and *X. laevis*, during embryogenesis.

Pregnant C57BL/6 mice were injected daily from gestational d 12–18 with TBT (0.05 or 0.5 mg/kg body weight ip) dissolved in sesame oil or vehicle alone. Pups were then killed at birth, and histological sections were prepared from liver, testis, mammary gland, and inguinal adipose tissue. Sections were stained

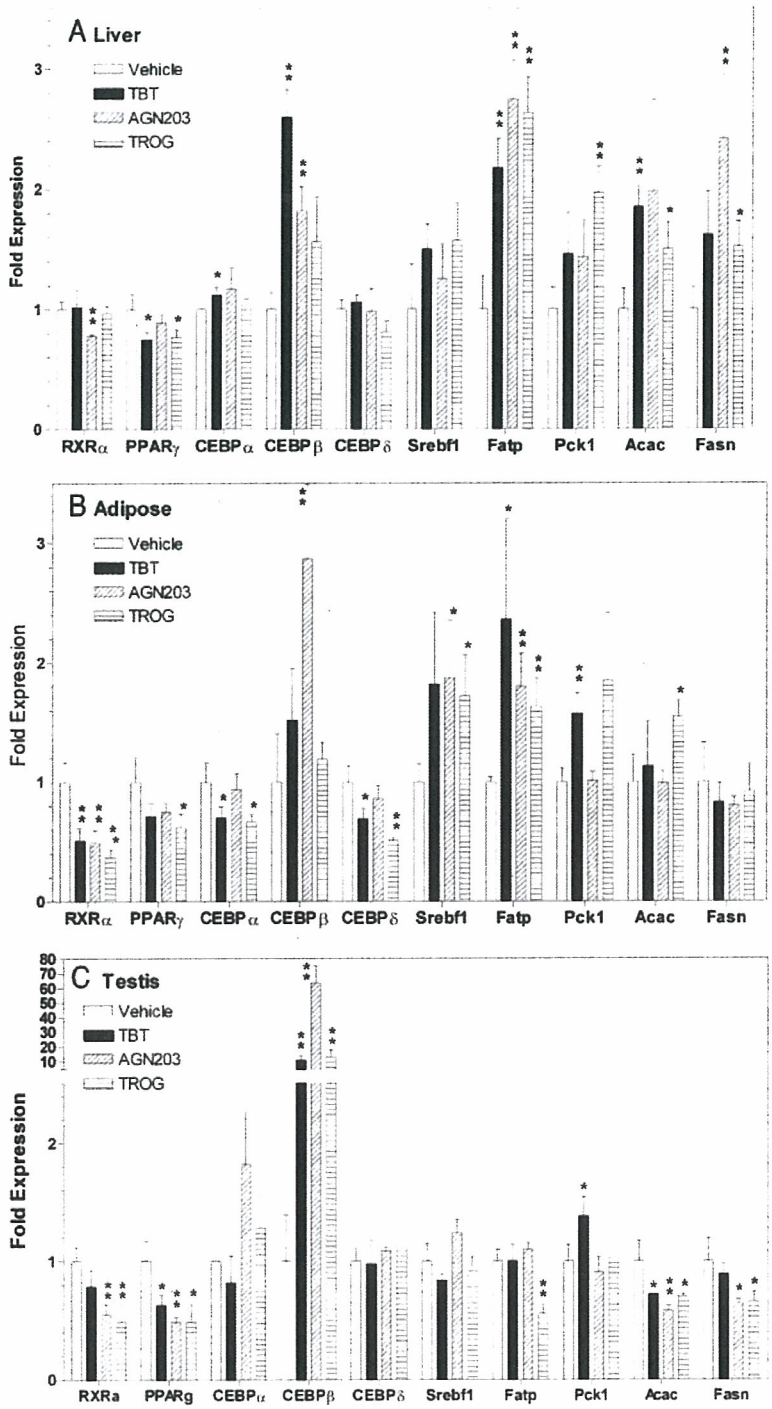

Fig. 3. *In Vivo* Induction of Adipogenic Modulators and RXR:PPARγ Target Genes

C57BL/6 male mice (three animals per treatment) were dosed with TBT (0.3 mg/kg b.w.), AGN195203 (0.3 mg/kg), troglitazone (3 mg/kg b.w.), or vehicle (corn oil) only by ip injection. Animals were killed after 24 h and dissected and cDNA was prepared from liver, epididymal fat pad, or testis for quantitative real-time PCR analysis. Expression levels were normalized to histone Hist2h4 and shown as the average fold change ± SEM (n = 3) compared with vehicle (corn oil) controls. Control *vs.* ligand treatments were analyzed by the unpaired Student's *t* test: *, $P < 0.1$; **, $P < 0.05$. TROG, Troglitazone.

with Oil Red O to assess changes in total tissue lipid accumulation. TBT exposure caused a disorganization of hepatic (Fig. 4, A and B) and gonadal (Fig. 4, C and D) architecture and significantly increased Oil Red O staining in treated animals *vs.* controls. Liver sections exhibited signs of steatosis consistent with the mis-

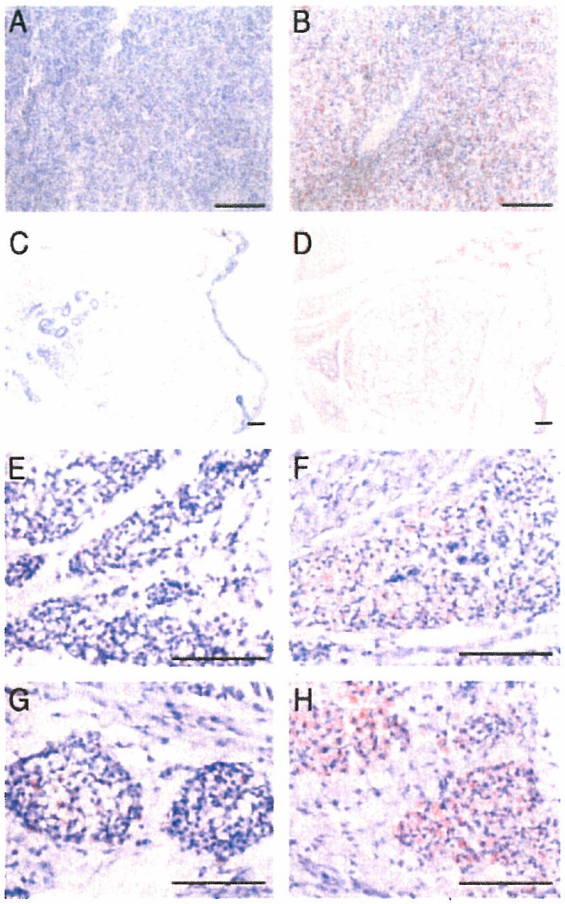

Fig. 4. *In Utero* Exposure to TBT Increases Adiposity in Mouse Liver, Testis, and Adipose Depots

Histological sections (12 μm) of newborn mouse liver (A and B), testis (C and D), inguinal adipose (E and F) and mammary adipose (G and H) stained with Oil Red O and counterstained with hematoxylin following *in utero* exposure to vehicle only (sesame oil) (A, C, E, and G) or 0.5 mg/kg b.w. TBT (B, D, F, and H) given s.c. daily from E12–18. *Scale bar*, 100 μm.

regulation of fatty acid uptake and synthesis observed using molecular markers. In addition, Oil Red O positive staining in mammary and inguinal adipose (Fig. 4, E–H) tissues was dramatically elevated, reflecting either an increase in lipid accumulation or an increase in mature adipocytes.

To determine whether exposure induced long-term changes in growth or adipose tissue, we followed mice from birth to adulthood after *in utero* exposure to TBT as indicated above. At birth, mice were cross-fostered to unexposed dams, and total body weight was recorded until 10 wk of age (Fig. 5A). Growth curves for male and female pups showed a slight trend for lower total body weight consistent with published observations (9) but were not statistically significant at 10 wk [control *vs.* TBT: male, 26.00 g ± 0.70 (n = 9) *vs.* 25.53 g ± 0.39 (n = 10), $P = 0.583$; female, 21.22 g ± 0.41 (n = 10), *vs.* 20.24 g ± 0.24 (n = 10), $P = 0.0529$]. Males were killed at 10 wk and epididymal fat pads were weighed (Fig. 5B). Adipose mass in TBT-treated males was increased significantly by 20% over controls [control *vs.* TBT: 0.30 g ± 0.020 (n = 9) *vs.* 0.36 g ± 0.018 (n = 10), $P = 0.0374$]. These data support the conclusion that TBT can increase body adiposity without overtly increasing total body weight. Similar lipid accumulation and changes in adipose tissue mass have also been observed after TZD or rexinoid treatment (55–57).

We had previously observed that TBT activated *Xenopus* RXRs (Table 1) and reasoned that the strong conservation in vertebrate nuclear receptor signaling pathways should result in consistent responses to organotin and RXR/PPARγ ligands across diverse vertebrate species. We therefore tested chronic exposure to environmentally relevant low doses of TBT (1–10 nM), the RXR-specific ligands LG100268 and AGN195203 (10–100 nM), troglitazone (0.1–1 μM), and estradiol (1–10 nM) on developing *X. laevis* tadpoles from stage 48 to metamorphs. To determine the effectiveness of these doses in *X. laevis* tadpoles, we used aromatase expression as a molecular marker because activity and expression are sensitive to endocrine disruption by organotins and RXR/PPARγ ligands in mammals (17, 18). *Xenopus* aromatase expression was similarly repressed 2- to 3-fold by 10 nM TBT, AGN195203, LG100268, or 1 μM troglitazone at stage 56 tadpoles (Fig. 6A) and at all subsequent stages. Despite significant ligand-induced aromatase down-regulation, neither sex ratios nor the time required to reach metamorphosis was altered (data not shown). *Xenopus* liver and kidney also exhibited no gross structural abnormalities at the doses given.

However, consistent with the testis and adipose results from mice presented above, we observed a dose-dependent increase in ectopic adipocyte formation posterior to the fat bodies in and around the gonads of both sexes after TBT or RXR/PPARγ ligand exposure (Fig. 6B). In contrast, estradiol-treated animals did not show increased adipocyte formation compared with controls. At 10 nM TBT, 10 nM AGN195203, or 1 μM troglitazone, ectopic adipocytes were observed in approximately 45–60% of animals. At the highest dose of TBT in males, testicular tissue was interspersed with, or replaced by, adipocytes along the anterior-posterior axis (Fig. 6, D, E, and G).

The concordant changes observed in *Xenopus* aromatase expression, gonadal adipocyte formation, and increased murine adiposity after exposure to TBT, RXR and PPARγ ligands are therefore consistent with a common mechanism of action through RXR:PPARγ activation, supporting the conclusion that endocrine disruption via nuclear receptor transcriptional regulation is a novel and key feature of organotin toxicity.

DISCUSSION

We have shown above that TBT is a potent inducer of adipogenesis, *in vitro* and *in vivo*, by acting as a novel,

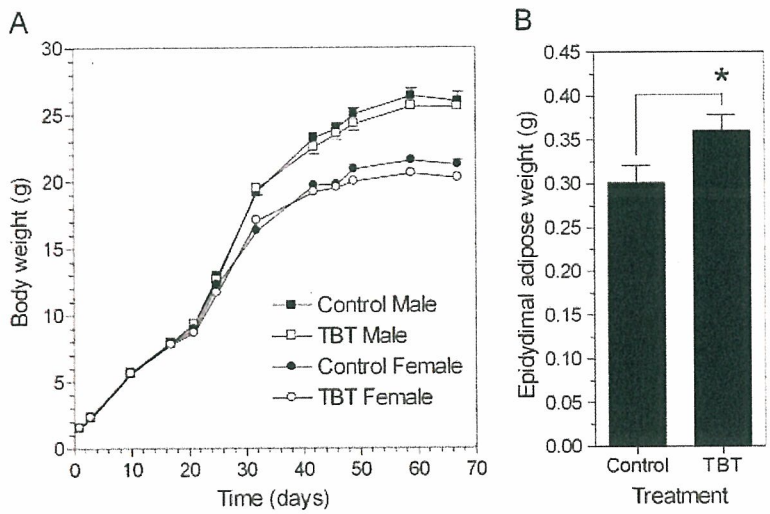

Fig. 5. *In Utero* Exposure to TBT Increases Adipose Mass But Not Body Weight in Adult Mice

A, Growth curves of C57BL/6 male and female pups exposed to control (sesame oil) or TBT *in utero* (E12–18). Data are mean ± SEM (n = 10). B, Epididymal fat pad weights from control or TBT-treated males at 10 wk. *, Epididymal adipose mass from exposed males was approximately 20% greater [control *vs.* TBT: 0.30 g ± 0.020 (n = 9) *vs.* 0.36 g ± 0.018 (n = 10); *, $P = 0.0374$). Data represent mean ± SEM (n = 9–10).

high-affinity xenobiotic ligand for RXRα and PPARγ. The ability of organotins to bind and activate these receptors, in particular the RXRs, which exhibit very restricted ligand specificity, is unexpected given the radically different chemical composition and three-dimensional molecular structure of organotins when compared with known natural and synthetic nuclear receptor ligands. Typically, RXR ligands comprise a carboxylic acid functional group and a three-dimensional molecular shape that mimics 9-*cis* RA. Structure-activity profiles indicate distinct structural preferences for organotins but also a relatively broad accommodation for agonist activity that is not easily reconciled with the classical ligand-binding model. Organotins may therefore interact somewhat differently than previously described RXR/PPARγ ligands with receptor LBDs to induce productive conformational changes required for coactivator recruitment. However, the binding data indicate that TBT is a potent and efficacious ligand for both RXRs and PPARγ that interacts, at least partially, with the same receptor-binding sites of other high-affinity ligands and promotes the necessary cofactor interactions required for agonist activation. In the study of Kanayama *et al.* (24), TBT was only effective in coactivator recruitment assays with PPARγ above 10 μM *in vitro*. However, in accord with our findings, they show that TBT activated PPARγ significantly at nanomolar concentrations in transfection assays. This may reflect a limitation of preference in the cofactor used *in vitro*. Alternatively, the lower maximal activation observed with TBT on PPARγ in cells (~30% at 100 nM TBT cf troglitazone) is consistent with one of two possibilities: either nonspecific cellular toxicity at high levels or activation as a partial agonist.

The ability of TBT to act as a dual ligand for permissive heterodimers such as RXRα:PPARγ, which can be activated by specific ligands for either receptor, also raises the possibility for additive or synergistic effects that might increase the potency of these compounds *in vivo* at low doses for this specific signaling pathway. Of note is that receptor activation is observed at nanomolar concentrations, whereas other mechanisms of toxicity and endocrine disruption, *e.g.* direct inhibition of aromatase activity, typically occur in the micromolar range. Furthermore, the activation of other permissive RXR heterodimeric partners, *e.g.* LXR and NURR1, suggests that organotins may act more widely to disrupt multiple nuclear receptor-mediated hormonal signaling pathways.

The biological consequences of organotin activation of the RXR:PPARγ signaling pathway are predictable and should follow known aspects of RXR/PPARγ biology. The RXR:PPARγ pathway plays a key role in adipocyte differentiation and energy storage, and is central to the control of whole-body metabolism (58). PPARγ activation increases the expression of genes that promote fatty acid storage and represses genes that induce lipolysis in adipocytes in white adipose tissue (59). PPARγ such as the thiazolidinediones can modulate insulin sensitivity due to these effects on the adipocyte, reversing insulin resistance in the whole body by sensitizing the muscle and liver tissue to insulin (60). However, a consequence of this increase in whole-body insulin sensitivity is that fat mass is increased through the promotion of triglyceride storage in adipocytes. Evidence is also mounting that depot-specific remodeling and adipocyte numbers increase after thiazolidinedione treatment (55–57). Therefore, PPARγ agonists comprise a class of phar-

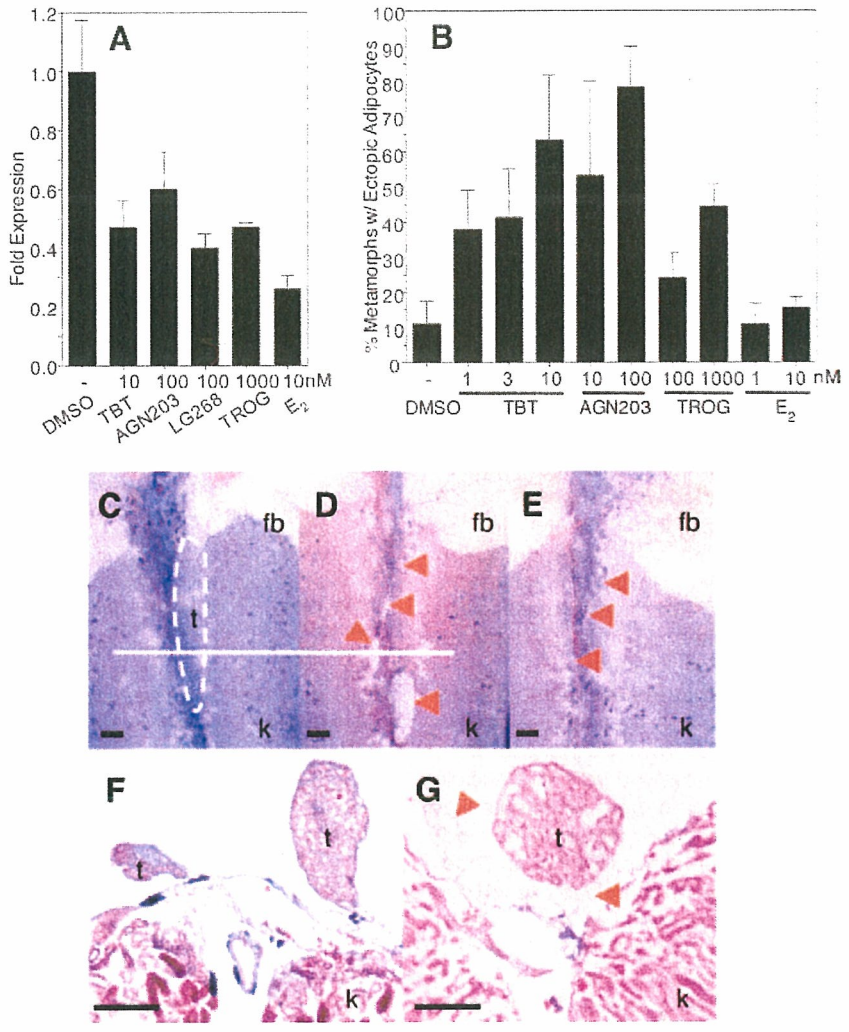

Fig. 6. Endocrine Disruption of RXR:PPARγ Signaling and Ectopic Induction of Adipocytes in *X. laevis* by TBT

A, Expression levels of *Xenopus* aromatase (XCYP19) were determined in tadpoles (stage 56) by quantitative real-time PCR after 24-h exposure to vehicle only (DMSO) or the indicated ligands. Expression was normalized to *Xenopus* EF1α and expressed as average fold change in expression ± SEM (n = 9) relative to vehicle controls. B, *X. laevis* tadpoles were dosed weekly under static renewal conditions with indicated ligands from stage 48 (before gonadogenesis) until stage 64 (metamorphic climax). Metamorphs (stage 66) were scored for ectopic adipocyte patches on gonads and urogenital ducts. Data are shown as the percentage of metamorphs exhibiting ectopic adipocyte patches posterior to the fat bodies; mean ± SD from triplicate tanks. C–E, Dissecting microscope photographs of kidneys (k), testis (t), and fat bodies (fb) from DMSO control, 10 nM TBT, and 1 μM troglitazone-treated male metamorphs. Multiple ectopic adipocyte patches (*red arrows*) are present posterior to the fat bodies along the anterior-posterior axis of gonads in TBT (D)- and troglitazone (E)-treated animals but not controls (C). Histological sections of kidneys and gonads from the same control (F) and 10 nM TBT (G)-treated males at the level indicated by the *white line* in C and D. Gonadal and connective tissue was either completely replaced by, or interspersed with, adipocytes (*red arrows*) in TBT-treated animals. Sections were developed with Mallory's trichrome stain. *Scale bars*, 100 μm.

maceutical therapies for type 2 diabetes that can also promote obesity by increasing fat storage. Likewise, RXR ligands also act as insulin-sensitizing agonists in rodents (61), underscoring the permissive nature of the PPARγ:RXR heterodimer and the potential effects on diabetes and obesity of both PPARγ and RXR agonists.

Our data are consistent with recent studies that organotins can mediate some of their endocrine disruption effects by transcriptional regulation through nuclear receptors, in particular RXR:PPARγ signaling (17–19, 24). Consequently, TBT exposure can promote adipocyte differentiation in the same manner as other RXR or PPARγ ligands *in vitro* using the standard murine 3T3-L1 cell model and *in vivo* through increased adiposity after intrauterine organotin exposure in newborn mice. It is currently unknown whether the increased adiposity *in vivo* results from an increase

in adipocyte precursor cell number, enhanced adipocyte differentiation from the same number of precursors, an increase in adipocyte size without an increase in number, or some combination of these.

The prevailing epidemiological data ascribe high-density caloric and/or fatty diets coupled with decreased physical activity as the root causes for the rise in obesity rates in the general population (62). The contribution of genetic components is less clear. Although genetic variation contributes to an individual's propensity to develop obesity, the rapid worldwide increase in obesity suggests that interaction with the modern environment exposes inherent genetic differences. The Barker hypothesis postulates that *in utero* fetal nutritional status is a potential risk factor for metabolic syndrome diseases (63–67). In this view, developmental metabolic programming of a thrifty phenotype limits the range in adaptive responses to the environment, *e.g.* diet and exercise, in later life (68). Experimental evidence from animal models lends support to this hypothesis (69). Plausible mechanisms include imprinting of obesity-sensitive hormonal pathways or changes in cell type and number, *e.g.* adipocytes, established during development.

Others, however, argue that the environment plays another role in obesity. Because the increase in obesity rates parallels the rapid growth in the use of industrial chemicals over the past 40 yr, it is plausible and provocative to associate *in utero* or chronic lifetime exposure to chemical triggers present in the modern environment with this epidemic. Hence, an "obesogen" model predicts the existence of xenobiotic chemicals that inappropriately regulate lipid metabolism and adipogenesis to promote obesity. Several recent studies serve as proof-of-principle for such a hypothesis. Environmental estrogens such as bisphenol A and nonylphenol, for instance, can promote adipocyte differentiation or proliferation in murine cell lines (70, 71). Furthermore, epidemiological studies link maternal smoking during pregnancy to an elevated risk of childhood obesity (72–76).

Seen in this context, we propose that organotins such as TBT and its congeners are chemical stressors or obesogens that activate RXR:PPARγ signaling to promote long-term changes in adipocyte number and/or lipid homeostasis after developmental or chronic lifetime exposure.

MATERIALS AND METHODS

Plasmids and Transfections

pCMX-GAL4 and pCMX-VP16 plasmid fusion constructs to nuclear receptor LBDs and coactivators [GAL4-hRARα, hRXRα, -xRXRα/γ, -hPPARγ, -mPPARα, -human steroid and xenobiotic receptor (SXR), -NURR1, -VDR, -LXR, -hACTR, -hPPAR-binding protein (PBP), -human steroid receptor coactivator-1 (SRC-1), human transcriptional intermediary factor 2 (TIF2)] have been previously described (77–82). Transfections were performed in Cos7 cells (transformed green monkey kidney fibroblast cell line) essentially as described elsewhere (83) using MH200-x4-TK-Luc as reporter and normalized to pCMX-β-galactosidase controls. Briefly, Cos7 cells were seeded at 5000 cells per well in 96-well tissue culture plates in 10% fetal bovine serum/DMEM and transfected for 8 h with 11 μg/plate of DNA/calcium phosphate precipitate mix (MH200x4-TK-Luc-CMX-β-galactosidase-nuclear receptor/coactivator effector(s) at a ratio of 5:5:1). Cells were washed free of precipitate with PBS and media were replaced with serum-free insulin, transferrin, lipid, bovine serum albumin supplemented (ITLB)/DMEM (84) plus ligands for an additional 24 h before assays for luciferase and β-galactosidase activity. All transfection data points were performed in triplicate, and all experiments were repeated at least three times.

Quantitative Real-Time PCR Analyses

Total cellular RNA from C57BL/6 mouse and *X. laevis* tissues was isolated with Trizol reagent and reversed transcribed with oligo dT and Superscript II (Invitrogen, San Diego, CA) according to the manufacturer's instructions. Triplicate cDNA samples (50 ng/reaction) were analyzed by quantitative real-time PCR on a DNA Engine Opticon thermal cycler [MJ Research (Watertown, MA)/Bio-Rad Laboratories (Hercules, CA)] using SYBR Green chemistry (PerkinElmer Life Sciences, Wellesley, MA). Fold changes in expression levels were calculated after normalization to histone Hist2h4 using the Δ-Δ cycle threshold method (85). Gene-specific primers were as follows. Hist2h4 forward (F): 5′-CCCGTGGTGTGCTGAAGGTGTT-3′; reverse (R), 5′-GAATTGAAGCGGCGGCGTCTA-3′; RXRα F: 5′-CGGCTGCTCAGGGTACTTGTGTTT-3′; R, 5′-CGGCTGCTCAGGGTACTTGTGTTT-3′; PPARγ F: 5′-TGGGTGAAACTCTGGGAGATTC-3′; R, 5′-AATTTCTTGTGAAGTGCTCATAGGC-3′; C/EBPα F: 5′-CCAAGAAGTCGGTGGACAAGA-3′; R, 5′-CGGTCATTGTCACTGGTCAACT-3′; C/EBPβ F: 5′-GCCCGCCGCCTTTAGACC-3′; R, 5′-CGCTCGTGCTCGCCAATG-3′; C/EBPδ F: 5′-AACCCGCGGCCTTCTACGAG-3′; R, 5′-ACGGCGGCCATGGAGTCAAT-3′; aP2 F: 5′-GAATTCGATGAAATCACCGCA-3′; R, 5′-CTCTTTATTGTGGTCGACTTTCCA-3′; FATP F: 5′-AGCCGCTTCTGGGATGACTGTGT-3′; R, 5′-ACCGAAGCGCTGCGTGAACTC-3′; ACS F: 5′-CCCAGCCAGTCCCCACCAG-3′; R, 5′-CACACCACTCAGGCTCACACTCGT-3′; FASN F: 5′-TCGGGTGTGGTGGGTTTGGTGAAT-3′; R, 5′-ACTTGGGGGCGTGAGATGTGTTGC-3′;ACAC F: 5′-G GATGGCAGCTCTGGAGGTGTATG-3′; R, 5′-TGTCCTTAAGCTGGCGGTGTTGTA; Pck1 F: 5′-CTGGCAGCATGGGGTGTTTGTAGG-3′; R, 5′-TGCCGAAGTTGTAGCCGAAGAAGG-3′; Srebf1 F: 5′-GCCCCTGCCCACCTCAAACCT-3′; R, 5′-ACTGGCACGGGCATCCTTCCTC-3′; *Xenopus* EF1α F: 5′-GATCCCAGGAAAGCCAATGTGC 3′; R, 5′-CCGGATCCTGCTGCCTTCTTCT-3′; *Xenopus* CYP19 (aromatase) F: 5′-GTCTGGATTAATGGCGAGGAAACA-3′; R, 5′-CTGATGAAGTATGGCCGAATGACC-3′.

Ligand Binding

Histidine-tagged RXRα LBD (H_6-RXRα LBDs) was expressed and purified from pET15b(+) vector in BL21(DE3) pLysS bacteria cultures after induction with 1 mM isopropyl-β-D-thiogalactopyranoside for 3 h at 37 C (86). Purified H_6-PPARγ was purchased from Invitrogen. Proteins were bound to 96-well Nickel Chelate Flashplates (PerkinElmer Life Sciences) at 100 μg/ml overnight at 4 C and washed five times with 200 μl/well Flashplate Assay Buffer (20 mM HEPES, pH 7.9; 100 mM KCl, 0.1% cholamidopropyldimethylammonio-2-hydroxy-1-propanesulfonate, 0.1 mM dithiothreitol). Competition assays typically used 1–5 nM [^{3}H]-9-*cis*-RA (PerkinElmer Life Sciences) or 10–50 nM [^{3}H]rosiglitazone (American Radiochemicals, Inc., St. Louis, MO) plus cold competitor ligands in Flashplate Assay Buffer at concentrations indicated in the figures. Plates were incubated at room temperature, pro-

tected from light, and read after 4 h on a Packard Topcount scintillation counter (Packard Instruments, Meriden, CT). Specific bound counts/min were determined by subtraction of counts/min from uncoated wells at each ligand concentration. Data were analyzed with GraphPad Prism 4.0 (GraphPad Software, Inc., San Diego, CA) using a one-site competition binding equation to determine K_i values for competitor ligands; K_d values of 1.4 and 41 nM for 9-*cis*-RA and rosiglitazone for their respective receptors were used in the calculations (87, 88).

3T3-L1 Cell Assays

3T3-L1 (American Type Culture Collection, Manassas, VA) cells were maintained as subconfluent cultures by passage every 3 d from cultures seeded at 5000 cells/cm^2 in 8% calf serum/DMEM. For differentiation assays, cells were seeded at 15×10^3 cells per well into 24-well tissue culture plates in 8% fetal bovine serum/DMEM, after which cultures were grown for 2 d and then treated with the indicated RXR, RAR, and PPAR ligands either with or without MDIT (100 μM 3-isobutyl-1-methylxanthine, 100 nM dexamethasone, 0.1 ng/ml insulin, and 2 nM T_3 thyroid hormone) induction cocktail. Media and ligand treatments were renewed every 2 d. After 1 wk, cells were scored for adipocyte differentiation by Oil Red O staining for lipid droplet accumulation. Cultures were washed with PBS, fixed with 10% formaldehyde for 15 min, washed with distilled water, and stained with filtered Oil Red O solution (4 g/liter, 60% isopropanol) for 15 min. Excess stain was removed by washing three times with distilled water. Three random fields from each well were photographed under phase contrast and analyzed in ImageJ. Images were converted into high-contrast black and white images to visualize lipid droplets and scored as the percentage area per field. Data are shown as the mean ± SEM from three wells per treatment. The method was validated by extraction of Oil Red O from stained cells into 100% isopropanol and quantitated by absorbance at 540 nm on a spectrophotometer.

In Vivo Animal Exposure Experiments

C57BL/6J mice were housed under a 12-h light, 12-h dark cycle. Pregnant mice were dosed by ip injection with TBT [0.05 or 0.5 mg/kg body weight (b.w.)] or vehicle (sesame oil) from embryonic d 12 (E12) every 24 h until the day before delivery. Neonates were killed at the day of delivery and analyzed. The samples were embedded in optimal cutting temperature embedding compound and sectioned (12 mm) using a cryostat. Sections were fixed on slides with 4% paraformaldehyde for 10 min and rinsed in PBS. The slides were then sequentially washed with distilled water and 60% of isopropanol and stained with Oil Red O (4 g/liter, 60% isopropanol). After washing with 60% isopropanol and distilled water, the slides were counterstained with hematoxylin. Sections were evaluated and photographed using a Zeiss microscope (Carl Zeiss, Thornwood, NY).

For long-term growth studies, pups were cross-fostered to unexposed C57BL/6 dams after birth, and litter sizes were kept constant at eight pups per dam (control, two male + two female; TBT treated, two male + two female). Animals were weaned at 3 wk of age and maintained on standard rodent chow. Total body weight was followed until 10 wk of age. Males were then killed, and epididymal fat pads were dissected and weighed.

X. laevis tadpoles were sorted at stage 48 (89) and maintained in 1-liter glass tanks in 20% Holtfreter's buffered salt solution (90) at a density of 10 tadpoles per tank on a diet of ground Tetramin Fish Flakes and spirulina. Compounds prepared in dimethylsulfoxide (DMSO) as 10^5-fold stock solutions were tested on triplicate tanks and dosed by static renewal after weekly water changes. Metamorphs at stage 64 were transferred to individual containers and fed frozen brine shrimp for 2 wk until stage 66. Froglets were euthanized with 250 mg/liter MS222 in 20% Holtfreter's solution and then scored for gonadal abnormalities and interrenal/gonadal adipocyte formation under a dissecting microscope. Kidneys with attached gonads and livers were fixed in 10% formalin-PBS, embedded in paraffin, and sectioned at 15 μm thickness. Sections were developed with Mallory's trichrome stain.

All animal experiments were approved and performed in accordance with Institutional Animal Care and Use Committee protocols.

Acknowledgments

We thank Drs. I. Blitz, K. Cho, C. Zhou, and T. Osborne for critical reading and comments on the manuscript, Dr. C. Li (Expression Technologies) for the H_6-RXRα LBD construct, and Dr. R. Chandraratna (Allergan Pharmaceuticals, Irvine, CA) for AGN203 and LG268).

Received September 8, 2005. Accepted March 30, 2006.

Address all correspondence and requests for reprints to: Bruce Blumberg, Department of Developmental and Cell Biology, University of California Irvine, 2113 McGaugh Hall, Irvine, California 92697-2300. E-mail: blumberg@uci.edu.

This work was supported by grants from the U.S. Environmental Protection Agency (STAR R830686) and National Institutes of Health (GM-60572) (to B.B.); from the Ministries of Education, Culture, Sports, Science and Technology, Environment and Health Labor and Welfare, Japan (to T.I.); and from the University of California Toxic Substance Research and Training Program (UC-37579) (to F.G.).

F.G., H.W., Z.Z., L.M., K.A., R.C., D.M.G., J.K., T.I. have nothing to declare. B.B. is a named inventor on U.S. patents US 5,861,274, US 6,200,802, and US 6,815,168.

REFERENCES

1. Appel KE 2004 Organotin compounds: toxicokinetic aspects. Drug Metab Rev 36:763–786
2. Golub M, Doherty J 2004 Triphenyltin as a potential human endocrine disruptor. J Toxicol Environ Health B Crit Rev 7:281–295
3. Blaber SJM 1970 The occurrence of a penis-like outgrowth behind the right tentacle in spent females of *Nucella lapillus*. Proc Malacolog Soc London 39:231–233
4. Gibbs P, Bryan G 1986 Reproductive failure in populations of the dog-whelk, *Nucella lapillus*, caused by imposex induced by tributyltin from antifouling paints. J Mar Biol Assoc UK 66:767–777
5. Matthiessen P, Gibbs P 1998 Critical appraisal of the evidence for tributyltin-mediated endocrine disruption in mollusks. Environ Toxicol Chem 17:37–43
6. Shimasaki Y, Kitano T, Oshima Y, Inoue S, Imada N, Honjo T 2003 Tributyltin causes masculinization in fish. Environ Toxicol Chem 22:141–144
7. McAllister BG, Kime DE 2003 Early life exposure to environmental levels of the aromatase inhibitor tributyltin causes masculinisation and irreversible sperm damage in zebrafish (*Danio rerio*). Aquat Toxicol 65:309–316
8. Omura M, Ogata R, Kubo K, Shimasaki Y, Aou S, Oshima Y, Tanaka A, Hirata M, Makita Y, Inoue N 2001 Two-generation reproductive toxicity study of tributyltin chloride in male rats. Toxicol Sci 64:224–232
9. Ogata R, Omura M, Shimasaki Y, Kubo K, Oshima Y, Aou S, Inoue N 2001 Two-generation reproductive toxicity

study of tributyltin chloride in female rats. J Toxicol Environ Health A 63:127–144
10. Boyer IJ 1989 Toxicity of dibutyltin, tributyltin and other organotin compounds to humans and to experimental animals. Toxicology 55:253–298
11. Heidrich DD, Steckelbroeck S, Klingmuller D 2001 Inhibition of human cytochrome P450 aromatase activity by butyltins. Steroids 66:763–769
12. Cooke GM 2002 Effect of organotins on human aromatase activity in vitro. Toxicol Lett 126:121–130
13. Powers MF, Beavis AD 1991 Triorganotins inhibit the mitochondrial inner membrane anion channel. J Biol Chem 266:17250–17256
14. Gennari A, Viviani B, Galli CL, Marinovich M, Pieters R, Corsini E 2000 Organotins induce apoptosis by disturbance of [Ca(2+)](i) and mitochondrial activity, causing oxidative stress and activation of caspases in rat thymocytes. Toxicol Appl Pharmacol 169:185–190
15. Philbert MA, Billingsley ML, Reuhl KR 2000 Mechanisms of injury in the central nervous system. Toxicol Pathol 28:43–53
16. Mu YM, Yanase T, Nishi Y, Waseda N, Oda T, Tanaka A, Takayanagi R, Nawata H 2000 Insulin sensitizer, troglitazone, directly inhibits aromatase activity in human ovarian granulosa cells. Biochem Biophys Res Commun 271:710–713
17. Mu YM, Yanase T, Nishi Y, Takayanagi R, Goto K, Nawata H 2001 Combined treatment with specific ligands for PPARγ:RXR nuclear receptor system markedly inhibits the expression of cytochrome P450arom in human granulosa cancer cells. Mol Cell Endocrinol 181:239–248
18. Saitoh M, Yanase T, Morinaga H, Tanabe M, Mu YM, Nishi Y, Nomura M, Okabe T, Goto K, Takayanagi R, Nawata H 2001 Tributyltin or triphenyltin inhibits aromatase activity in the human granulosa-like tumor cell line KGN. Biochem Biophys Res Commun 289:198–204
19. Nishikawa J, Mamiya S, Kanayama T, Nishikawa T, Shiraishi F, Horiguchi T 2004 Involvement of the retinoid X receptor in the development of imposex caused by organotins in gastropods. Environ Sci Technol 38: 6271–6276
20. Baillie-Hamilton PF 2002 Chemical toxins: a hypothesis to explain the global obesity epidemic. J Altern Complement Med 8:185–192
21. Heindel JJ 2003 Endocrine disruptors and the obesity epidemic. Toxicol Sci 76:247–249
22. Jacobs MN, Lewis DF 2002 Steroid hormone receptors and dietary ligands: a selected review. Proc Nutr Soc 61:105–122
23. Watanabe H, Iguchi T, Morohashi K 2002 [Endocrine disruptors and nuclear receptors]. Nippon Rinsho 60: 397–403
24. Kanayama T, Kobayashi N, Mamiya S, Nakanishi T, Nishikawa J 2005 Organotin compounds promote adipocyte differentiation as agonists of the peroxisome proliferator-activated receptor γ/retinoid X receptor pathway. Mol Pharmacol 67:766–774
25. Wang Z, Benoit G, Liu J, Prasad S, Aarnisalo P, Liu X, Xu H, Walker NP, Perlmann T 2003 Structure and function of Nurr1 identifies a class of ligand-independent nuclear receptors. Nature 423:555–560
26. Aarnisalo P, Kim CH, Lee JW, Perlmann T 2002 Defining requirements for heterodimerization between the retinoid X receptor and the orphan nuclear receptor Nurr1. J Biol Chem 277:35118–35123
27. Boehm MF, Zhang L, Zhi L, McClurg MR, Berger E, Wagoner M, Mais DE, Suto CM, Davies JA, Heyman RA, Nadzant AM 1995 Design and synthesis of potent retinoid X receptor selective ligands that induce apoptosis in leukemia cells. J Med Chem 38:3146–3155
28. Yu C, Chen L, Luo H, Chen J, Cheng F, Gui C, Zhang R, Shen J, Chen K, Jiang H, Shen X 2004 Binding analyses between human PPARγ-LBD and ligands. Eur J Biochem 271:386–397
29. Forman BM, Tontonoz P, Chen J, Brun RP, Spiegelman BM, Evans RM 1995 15-Deoxy-δ 12, 14-prostaglandin J2 is a ligand for the adipocyte determination factor PPAR γ. Cell 83:803–812
30. Schoonjans K, Staels B, Auwerx J 1996 The peroxisome proliferator activated receptors (PPARs) and their effects on lipid metabolism and adipocyte differentiation. Biochim Biophys Acta 1302:93–109
31. Kersten S 2002 Peroxisome proliferator activated receptors and obesity. Eur J Pharmacol 440:223–234
32. Lane MD, Tang QQ, Jiang MS 1999 Role of the CCAAT enhancer binding proteins (C/EBPs) in adipocyte differentiation. Biochem Biophys Res Commun 266:677–683
33. Tang QQ, Otto TC, Lane MD 2003 CCAAT/enhancer-binding protein β is required for mitotic clonal expansion during adipogenesis. Proc Natl Acad Sci USA 100: 850–855
34. Tang QQ, Lane MD 1999 Activation and centromeric localization of CCAAT/enhancer-binding proteins during the mitotic clonal expansion of adipocyte differentiation. Genes Dev 13:2231–2241
35. Rubin CS, Hirsch A, Fung C, Rosen OM 1978 Development of hormone receptors and hormonal responsiveness in vitro. Insulin receptors and insulin sensitivity in the preadipocyte and adipocyte forms of 3T3–L1 cells. J Biol Chem 253:7570–7578
36. Kletzien RF, Clarke SD, Ulrich RG 1992 Enhancement of adipocyte differentiation by an insulin-sensitizing agent. Mol Pharmacol 41:393–398
37. Kletzien RF, Foellmi LA, Harris PK, Wyse BM, Clarke SD 1992 Adipocyte fatty acid-binding protein: regulation of gene expression in vivo and in vitro by an insulin-sensitizing agent. Mol Pharmacol 42:558–562
38. Tafuri SR 1996 Troglitazone enhances differentiation, basal glucose uptake, and Glut1 protein levels in 3T3–L1 adipocytes. Endocrinology 137:4706–4712
39. Xue JC, Schwarz EJ, Chawla A, Lazar MA 1996 Distinct stages in adipogenesis revealed by retinoid inhibition of differentiation after induction of PPARγ. Mol Cell Biol 16:1567–1575
40. Kawada T, Kamei Y, Sugimoto E 1996 The possibility of active form of vitamins A and D as suppressors on adipocyte development via ligand-dependent transcriptional regulators. Int J Obes Relat Metab Disord 20(Suppl 3):S52–S57
41. Kawada T, Kamei Y, Fujita A, Hida Y, Takahashi N, Sugimoto E, Fushiki T 2000 Carotenoids and retinoids as suppressors on adipocyte differentiation via nuclear receptors. Biofactors 13:103–109
42. Tontonoz P, Graves RA, Budavari AI, Erdjument-Bromage H, Lui M, Hu E, Tempst P, Spiegelman BM 1994 Adipocyte-specific transcription factor ARF6 is a heterodimeric complex of two nuclear hormone receptors, PPAR γ and RXR α. Nucleic Acids Res 22:5628–5634
43. Martin G, Schoonjans K, Lefebvre AM, Staels B, Auwerx J 1997 Coordinate regulation of the expression of the fatty acid transport protein and acyl-CoA synthetase genes by PPARα and PPARγ activators. J Biol Chem 272:28210–28217
44. Motojima K, Passilly P, Peters JM, Gonzalez FJ, Latruffe N 1998 Expression of putative fatty acid transporter genes are regulated by peroxisome proliferator-activated receptor α and γ activators in a tissue- and inducer-specific manner. J Biol Chem 273:16710–16714
45. Frohnert BI, Hui TY, Bernlohr DA 1999 Identification of a functional peroxisome proliferator-responsive element in the murine fatty acid transport protein gene. J Biol Chem 274:3970–3977
46. Martin G, Poirier H, Hennuyer N, Crombie D, Fruchart JC, Heyman RA, Besnard P, Auwerx J 2000 Induction of the fatty acid transport protein 1 and acyl-CoA synthase

genes by dimer-selective rexinoids suggests that the peroxisome proliferator-activated receptor-retinoid X receptor heterodimer is their molecular target. J Biol Chem 275:12612–12618
47. Tontonoz P, Hu E, Devine J, Beale EG, Spiegelman BM 1995 PPAR γ 2 regulates adipose expression of the phosphoenolpyruvate carboxykinase gene. Mol Cell Biol 15:351–357
48. Magana MM, Lin SS, Dooley KA, Osborne TF 1997 Sterol regulation of acetyl coenzyme A carboxylase promoter requires two interdependent binding sites for sterol regulatory element binding proteins. J Lipid Res 38: 1630–1638
49. Schadinger SE, Bucher NL, Schreiber BM, Farmer SR 2005 PPARγ2 regulates lipogenesis and lipid accumulation in steatotic hepatocytes. Am J Physiol Endocrinol Metab 288:E1195–E1205
50. Tontonoz P, Kim JB, Graves RA, Spiegelman BM 1993 ADD1: a novel helix-loop-helix transcription factor associated with adipocyte determination and differentiation. Mol Cell Biol 13:4753–4759
51. Kim JB, Spiegelman BM 1996 ADD1/SREBP1 promotes adipocyte differentiation and gene expression linked to fatty acid metabolism. Genes Dev 10:1096–1107
52. Joseph SB, Laffitte BA, Patel PH, Watson MA, Matsukuma KE, Walczak R, Collins JL, Osborne TF, Tontonoz P 2002 Direct and indirect mechanisms for regulation of fatty acid synthase gene expression by liver X receptors. J Biol Chem 277:11019–11025
53. Seo JB, Moon HM, Kim WS, Lee YS, Jeong HW, Yoo EJ, Ham J, Kang H, Park MG, Steffensen KR, Stulnig TM, Gustafsson JA, Park SD, Kim JB 2004 Activated liver X receptors stimulate adipocyte differentiation through induction of peroxisome proliferator-activated receptor γ expression. Mol Cell Biol 24:3430–3444
54. Yu S, Matsusue K, Kashireddy P, Cao WQ, Yeldandi V, Yeldandi AV, Rao MS, Gonzalez FJ, Reddy JK 2003 Adipocyte-specific gene expression and adipogenic steatosis in the mouse liver due to peroxisome proliferator-activated receptor γ1 (PPARγ1) overexpression. J Biol Chem 278:498–505
55. Hallakou S, Doare L, Foufelle F, Kergoat M, Guerre-Millo M, Berthault MF, Dugail I, Morin J, Auwerx J, Ferre P 1997 Pioglitazone induces in vivo adipocyte differentiation in the obese Zucker fa/fa rat. Diabetes 46:1393–1399
56. de Souza CJ, Eckhardt M, Gagen K, Dong M, Chen W, Laurent D, Burkey BF 2001 Effects of pioglitazone on adipose tissue remodeling within the setting of obesity and insulin resistance. Diabetes 50:1863–1871
57. Smith SR, De Jonge L, Volaufova J, Li Y, Xie H, Bray GA 2005 Effect of pioglitazone on body composition and energy expenditure: a randomized controlled trial. Metabolism 54:24–32
58. Auwerx J 1999 PPARγ, the ultimate thrifty gene. Diabetologia 42:1033–1049
59. Ferre P 2004 The biology of peroxisome proliferator-activated receptors: relationship with lipid metabolism and insulin sensitivity. Diabetes 53(Suppl 1):S43–S50
60. Day C 1999 Thiazolidinediones: a new class of antidiabetic drugs. Diabet Med 16:179–192
61. Mukherjee R, Davies PJ, Crombie DL, Bischoff ED, Cesario RM, Jow L, Hamann LG, Boehm MF, Mondon CE, Nadzan AM, Paterniti Jr JR, Heyman RA 1997 Sensitization of diabetic and obese mice to insulin by retinoid X receptor agonists. Nature 386:407–410
62. Hill JO, Peters JC 1998 Environmental contributions to the obesity epidemic. Science 280:1371–1374
63. Barker DJ, Bull AR, Osmond C, Simmonds SJ 1990 Fetal and placental size and risk of hypertension in adult life. Br Med J 301:259–262
64. Phillips DI, Hirst S, Clark PM, Hales CN, Osmond C 1994 Fetal growth and insulin secretion in adult life. Diabetologia 37:592–596
65. Martyn CN, Barker DJ, Jespersen S, Greenwald S, Osmond C, Berry C 1995 Growth in utero, adult blood pressure, and arterial compliance. Br Heart J 73:116–121
66. Yajnik C 2000 Interactions of perturbations in intrauterine growth and growth during childhood on the risk of adult-onset disease. Proc Nutr Soc 59:257–265
67. Barker DJ, Martyn CN, Osmond C, Hales CN, Fall CH 1993 Growth in utero and serum cholesterol concentrations in adult life. Br Med J 307:1524–1527
68. Lucas A 1998 Programming by early nutrition: an experimental approach. J Nutr 128:401S–406S
69. Armitage JA, Khan IY, Taylor PD, Nathanielsz PW, Poston L 2004 Developmental programming of metabolic syndrome by maternal nutritional imbalance; how strong is the evidence from experimental models in mammals? J Physiol 561:355–377
70. Masuno H, Kidani T, Sekiya K, Sakayama K, Shiosaka T, Yamamoto H, Honda K 2002 Bisphenol A in combination with insulin can accelerate the conversion of 3T3-L1 fibroblasts to adipocytes. J Lipid Res 43:676–684
71. Masuno H, Okamoto S, Iwanami J, Honda K, Shiosaka T, Kidani T, Sakayama K, Yamamoto H 2003 Effect of 4-nonylphenol on cell proliferation and adipocyte formation in cultures of fully differentiated 3T3-L1 cells. Toxicol Sci 75:314–320
72. Toschke AM, Koletzko B, Slikker Jr W, Hermann M, von Kries R 2002 Childhood obesity is associated with maternal smoking in pregnancy. Eur J Pediatr 161:445–448
73. von Kries R, Toschke AM, Koletzko B, Slikker Jr W 2002 Maternal smoking during pregnancy and childhood obesity. Am J Epidemiol 156:954–961
74. Oken E, Huh SY, Taveras EM, Rich-Edwards JW, Gillman MW 2005 Associations of maternal prenatal smoking with child adiposity and blood pressure. Obes Res 13: 2021–2028
75. Power C, Jefferis BJ 2002 Fetal environment and subsequent obesity: a study of maternal smoking. Int J Epidemiol 31:413–419
76. Hill SY, Shen S, Locke Wellman J, Rickin E, Lowers L 2005 Offspring from families at high risk for alcohol dependence: increased body mass index in association with prenatal exposure to cigarettes but not alcohol. Psychiatry Res 135:203–216
77. Umesono K, Murakami KK, Thompson CC, Evans RM 1991 Direct repeats as selective response elements for the thyroid hormone, retinoic acid, and vitamin D3 receptors. Cell 65:1255–1266
78. Perlmann T, Rangarajan PN, Umesono K, Evans RM 1993 Determinants for selective RAR and TR recognition of direct repeat HREs. Genes Dev 7:1411–1422
79. Blumberg B, Mangelsdorf DJ, Dyck JA, Bittner DA, Evans RM, De Robertis EM 1992 Multiple retinoid-responsive receptors in a single cell: families of retinoid "X" receptors and retinoic acid receptors in the *Xenopus* egg. Proc Natl Acad Sci USA 89:2321–2325
80. Blumberg B, Bolado J Jr., Derguini F, Craig AG, Moreno TA, Chakravarti D, Heyman RA, Buck J, Evans RM 1996 Novel retinoic acid receptor ligands in *Xenopus* embryos. Proc Natl Acad Sci USA 93:4873–4878
81. Blumberg B, Sabbagh Jr W, Juguilon H, Bolado Jr J, van Meter CM, Ong ES, Evans RM 1998 SXR, a novel steroid and xenobiotic-sensing nuclear receptor. Genes Dev 12: 3195–3205
82. Tabb MM, Sun A, Zhou C, Grun F, Errandi J, Romero K, Pham H, Inoue S, Mallick S, Lin M, Forman BM, Blumberg B 2003 Vitamin K2 regulation of bone homeostasis is mediated by the steroid and xenobiotic receptor SXR. J Biol Chem 278:43919–43927
83. Grun F, Blumberg B 2003 Identification of novel nuclear hormone receptor ligands by activity-guided purification. Methods Enzymol 364:3–24
84. Grun F, Venkatesan RN, Tabb MM, Zhou C, Cao J, Hemmati D, Blumberg B 2002 Benzoate X receptors α

and β are pharmacologically distinct and do not function as xenobiotic receptors. J Biol Chem 277:43691–43697
85. Livak KJ, Schmittgen TD 2001 Analysis of relative gene expression data using real-time quantitative PCR and the 2(-Δ Δ C(T)) method. Methods 25:402–408
86. Bourguet W, Ruff M, Chambon P, Gronemeyer H, Moras D 1995 Crystal structure of the ligand-binding domain of the human nuclear receptor RXR-α. Nature 375:377–382
87. Allegretto EA, McClurg MR, Lazarchik SB, Clemm DL, Kerner SA, Elgort MG, Boehm MF, White SK, Pike JW, Heyman RA 1993 Transactivation properties of retinoic acid and retinoid X receptors in mammalian cells and yeast. Correlation with hormone binding and effects of metabolism. J Biol Chem 268:26625–26633
88. Lehmann JM, Moore LB, Smith-Oliver TA, Wilkison WO, Willson TM, Kliewer SA 1995 An antidiabetic thiazolidinedione is a high affinity ligand for peroxisome proliferator-activated receptor γ (PPAR γ). J Biol Chem 270: 12953–12956
89. Nieuwkoop P, Faber J 1994 Normal table of *Xenopus laevis* (Daudin). 2nd ed. New York: Garland Publishing, Inc.
90. Rugh R 1962 Experimental embryology: techniques and procedures. 3rd ed. Minneapolis: Burgess Publishing Co.

Molecular Endocrinology **is published monthly by The Endocrine Society (http://www.endo-society.org), the foremost professional society serving the endocrine community.**

BMC Genomics

BioMed Central

Methodology article

Open Access

"Per cell" normalization method for mRNA measurement by quantitative PCR and microarrays

Jun Kanno*†[1], Ken-ichi Aisaki†[1], Katsuhide Igarashi[1], Noriyuki Nakatsu[1], Atsushi Ono[1], Yukio Kodama[1] and Taku Nagao[2]

Address: [1]Division of Cellular and Molecular Toxicology, National Institute of Health Sciences, 1-18-1, Kamiyoga, Setagaya-ku, Tokyo 158-8501, Japan and [2]President, National Institute of Health Sciences, 1-18-1, Kamiyoga, Setagaya-ku, Tokyo 158-8501, Japan

Email: Jun Kanno* - kanno@nihs.go.jp; Ken-ichi Aisaki - aisaki@nihs.go.jp; Katsuhide Igarashi - igarashi@nihs.go.jp; Noriyuki Nakatsu - n-nakatsu@nihs.go.jp; Atsushi Ono - Atsushi@nibio.go.jp; Yukio Kodama - kodama@nihs.go.jp; Taku Nagao - nagao@nihs.go.jp

* Corresponding author †Equal contributors

Published: 29 March 2006

*BMC Genomics*2006, **7**:64 doi:10.1186/1471-2164-7-64

Received: 06 November 2005
Accepted: 29 March 2006

This article is available from: http://www.biomedcentral.com/1471-2164/7/64

Abstract

Background: Transcriptome data from quantitative PCR (Q-PCR) and DNA microarrays are typically obtained from a fixed amount of RNA collected per sample. Therefore, variations in tissue cellularity and RNA yield across samples in an experimental series compromise accurate determination of the absolute level of each mRNA species per cell in any sample. Since mRNAs are copied from genomic DNA, the simplest way to express mRNA level would be as copy number per template DNA, or more practically, as copy number per cell.

Results: Here we report a method (designated the "Percellome" method) for normalizing the expression of mRNA values in biological samples. It provides a "per cell" readout in mRNA copy number and is applicable to both quantitative PCR (Q-PCR) and DNA microarray studies. The genomic DNA content of each sample homogenate was measured from a small aliquot to derive the number of cells in the sample. A cocktail of five external spike RNAs admixed in a dose-graded manner (dose-graded spike cocktail; GSC) was prepared and added to each homogenate in proportion to its DNA content. In this way, the spike mRNAs represented absolute copy numbers per cell in the sample. The signals from the five spike mRNAs were used as a dose-response standard curve for each sample, enabling us to convert all the signals measured to copy numbers per cell in an expression profile-independent manner. A series of samples was measured by Q-PCR and Affymetrix GeneChip microarrays using this Percellome method, and the results showed up to 90 % concordance.

Conclusion: Percellome data can be compared directly among samples and among different studies, and between different platforms, without further normalization. Therefore, "percellome" normalization can serve as a standard method for exchanging and comparing data across different platforms and among different laboratories.

Background

Normalization of gene expression data between different samples generated in the same laboratory using a single platform, and/or generated in different geographical

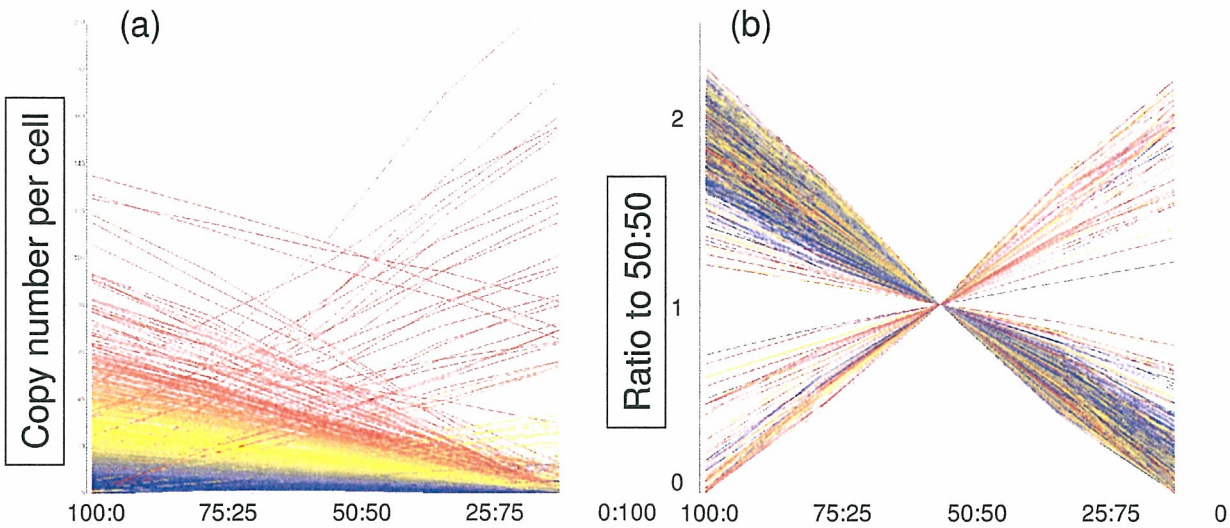

Figure 1
Dose-response linearity check by LBM. Dose-response linearity of the Affymetrix GeneChip by the LBM (liver-brain mix) sample set. Five samples, i.e. mixtures of mouse liver and brain at ratios of 100:0, 75:25, 50:50, 25:75 and 0:100, were spiked with GSC and measured by Affymetrix GeneChips Mouse430-2. Signals were normalized by the Percellome method as described in the text. Line graphs are in (a) copy numbers and (b) ratio to 50:50 sample for the top 1,000 probe sets with coefficient of correlation (R^2) closest to 1 among those having 1 copy or more per cell in the 50:50 sample (19,979 probe sets out of 45,101). The number of probe sets with $R^2 > 0.950$ was 8,655, and $R^2 > 0.900$ was 11,719.

regions using multiple platforms, is central to the establishment of a reliable reference database for toxicogenomics and pharmacogenomics. Transforming expression data into a "per cell" database is an effective way of normalizing expression data across samples and platforms. However, transcriptome data from the quantitative PCR (Q-PCR) and DNA microarray analyses currently deposited in the database are related to a fixed amount of RNA collected per sample. Variations in RNA yield across samples in an experimental series compromise accurate determination of the absolute level of each mRNA species per cell in any sample. Normalization against housekeeping genes for PCRs, and global normalization of ratiometric data for microarrays, is typically performed to account for this informational loss. Additional methods, such as the use of external mRNA spikes, reportedly improve the quality of data from microarray systems. For example, Holstege et al. [1] described a spike method against total RNA, based on their finding that the yields of total RNA from wild type and mutant cells were very similar. Hill et al. [2] reported a spike method against total RNA for normalizing hybridization data such that the sensitivities of individual arrays could be compared. Lee et al. [3] demonstrated that "housekeeping genes" cannot be used as a reference control, and van de Peppel et al. [4] described a normalization method of mRNA against total RNA using an external spike mixture. To achieve satisfactory performance they used multiple graded doses of external spikes, covering a wide range of expression, in order to align the ratiometric data by Lowess normalization [5]. Hekstra et al. [6] presented a method for calculating the final cRNA concentration in a hybridization solution. Sterrenburg et al. [7] and Dudley et al. [8] reported the use of common reference control samples for two-color microarray analyses of the human and yeast genomes, respectively. These are pools of antisense oligo sequences against all sense oligos present on the microarray. Instead of antisense oligos, Talaat et al. [9] used genomic DNA as a common reference control in studies of *E. coli*. Statistical approaches have been proposed for ratiometric data to improve inter-microarray variations, especially of non-linear relations [10]. However, because control samples may differ among studies, ratiometric data cannot easily be compared across multiple studies unless a common reference, such as a mixture of all antisense counterparts of spotted sense sequences is used [7-9]. Nevertheless, as long as the normalization is calibrated to total RNA, variations in total RNA profile cannot be effectively cancelled out. Although

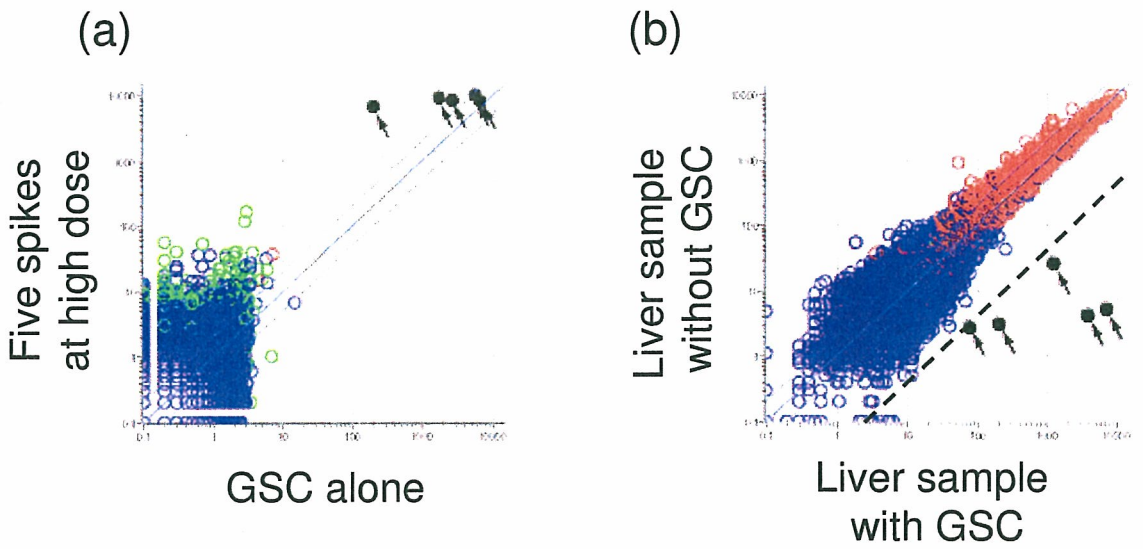

Figure 2
Cross-hybridization of GSC. Cross-hybridization of the GSC spike mRNAs to Affymetrix GeneChip. (a) A scatter plot of a blank sample with the GSC (horizontal axis) and a blank with the five spike RNAs at a high dosage (vertical axis) measured by MG-U74v2A GeneChips (raw values generated by Affymetrix MAS 5.0 software). The five spikes are indicated by black dots with arrows. Signals of the murine probe sets were below 20 on the horizontal axis, indicating negligible cross-hybridization of GSC spike mRNAs to the murine probe sets. (b) A scatter plot of a liver sample with GSC (horizontal axis) and without GSC (vertical axis) measured by MG-U74v2A GeneChips. The five spikes are again indicated by black dots with arrows. The dotted line is the 1/25 fold (4%) line. Cross-hybridization of mouse liver mRNAs to the GSC signals was considered negligible (less than 4%).

some of these reports share the idea that "absolute expression" and "transcripts per cell" should entail robust normalization, further practical development to enable universal application has been awaited.

Here, we report a method for normalizing expression data across samples and methods to the cell number of each sample, using the DNA content as indicator. This normalization method is independent of the gene expression profile of the sample, and may contribute to transcriptome studies as a common standard for data comparison and interchange.

Results

Dose-response linearity of the measurement system as a basis for the Percellome method

The fidelity of transcript detection is the key to this "per cell" based normalization method, which generates transcriptome data in "mRNA copy numbers per cell". The Q-PCR system was tested by serially diluting samples to confirm the linear relationship between Ct values and the log of sample mRNA concentration (data not shown). High density oligonucleotide microarrays from Affymetrix [11] were used in our experiments. We tested the linearity of the Affymetrix GeneChips using a set of five samples made of mixtures of liver and brain in ratios of 100:0, 75:25, 50:50, 25:75, and 0:100 (designated "LBM" for liver-brain mix). The results showed a linear relationship ($R^2 > 0.90$) between fluorescence intensity and input for a sufficient proportion of probe sets, i.e. about 37% of the probe sets in the older MG-U74v2 and 70% in the newest Mouse Genome 430 2.0 GeneChip were above the detection level (approximately one copy per cell) in the 50:50 sample (Figure 1) [see Additional files 1 and 2].

Dose-response linearity alone is not sufficient to generate true mRNA copy numbers. An important additional requirement is that the ratio of signal intensity to mRNA copy number should be equal among all GeneChip probe sets of mRNAs and PCR primers. The Q-PCR primer sets were designed to perform at similar amplification rates to minimize differences between amplicons. The melting

Table 1: The spike factors for various organs/tissues

Species	Organ/Tissue (adult, unless otherwise noted)	Spike Factor	total RNA/genomic DNA	SD
Mouse	Liver	0.2	211	46
Mouse	Lung	0.02	22	4
Mouse	Heart	0.05	-	-
Mouse	Thymus	0.01	8	2
Mouse	Colon Epitherium	0.05	105	30
Mouse	Kidney	0.1	-	-
Mouse	Brain	0.1	-	-
Mouse	Suprachiasmatic nucleus (SCN)	0.1	-	-
Mouse	Hypothalamus	0.1	63	4
Mouse	Pituitary	0.1	52	8
Mouse	Ovary	0.02	35	4
Mouse	Uterus	0.02	42	12
Mouse	Vagina	0.02	81	38
Mouse	Testis	0.15	56	7
Mouse	Epididymis	0.07	53	16
Mouse	Bone marrow	0.02	14	3
Mouse	Spleen	0.02	-	-
Mouse	Whole Embryo	0.15	97	36
Mouse	Fetal Telencephalon E10.5–16.5	0.1	48	9
Mouse	Neurosphere (E11.5–14.5)	0.03	42	10
Mouse	E9.5 embryo heart	0.15	58	15
Mouse	cell lines	0.2	-	-
Rat	Liver	0.2	-	-
Rat	Kidney	0.2	-	-
Rat	Uterus	0.04	56	5
Rat	Ovary	0.04	56	9
Human	Cancer Cell Lines	0.2	116	26
Xenopus	liver	0.03	-	-
Xenopus	embryo	0.15	-	-

temperature was set between 60° and 65°C with a product size of approximately 100 base pairs using an algorithm (nearest neighbor method, TAKARA BIO Inc., Japan), and the amplification co-efficiency (E) was set within the range 0.9 ± 0.1 (E = 2^{-(1/slope)}-1 on a plot of log2 (template) against Ct value). For the GeneChip system, the signal/copy performance of each probe set depended on the strategy of designing the probes to keep the hybridization constant/melting temperature within a narrow range, ensuring that the dose-response performances of the probe sets were similar (cf. http://www.affymetrix.com/technology/design/index.affx). Failing this, any differences should at least be kept constant within the same make/version of the GeneChip. Taking into consideration the biases that lead to imperfections in estimating absolute copy numbers in each gene/probe set, we developed normalization methods to set up a common scale for Q-PCR and Affymetrix GeneChip systems.

The grade-dosed spike cocktail (GSC) and the "spike factor" for the Percellome method

A set of external spike mRNAs was used to transfer the measurement of cell number in the sample (as reflected by its DNA content) to transcriptome analysis. For the spikes, we utilized five *Bacillus subtilis* mRNAs that were left open for users in the Affymetrix GeneChip series. The extent to which the *Bacillus* RNAs cross-hybridized with other probe sets was checked for the Affymetrix GeneChip system. The GSC was applied to Murine Genome U74Av2 Array (MG-U74v2) GeneChips with or without a liver sample. As shown in Figure 2, cross-hybridization between *Bacillus* RNAs and the murine gene probe sets was negligible [see Additional files 3 and 4]. Mouse Genome 430 2.0 Array (Mouse430-2), Mouse Expression Arrays 430A (MOE430A) and B (MOE430B), Rat Expression Array 230A (RAE230A), *Xenopus laevis* Genome Array and Human Genome U95Av2 (HG-U95Av2) and U133A (HG-U133A) Arrays sharing the same probe sets for these spike mRNAs showed no sign of cross-hybridization with the *Bacillus* probes (data not shown).

We prepared a cocktail containing in vitro transcribed Bacillus mRNAs in threefold concentration steps, i.e. 777.6 pM (for AFFX-ThrX-3_at), 259.4 pM (for AFFX-LysX-3_at), 86.4 pM (for AFFX-PheX-3_at), 28.8 pM (for AFFX-DapX-3_at) and 9.6 pM (for AFFX-TrpnX-3_at). By referring to the amount of DNA in a diploid cell and employing a "spike factor" determined by the ratio of

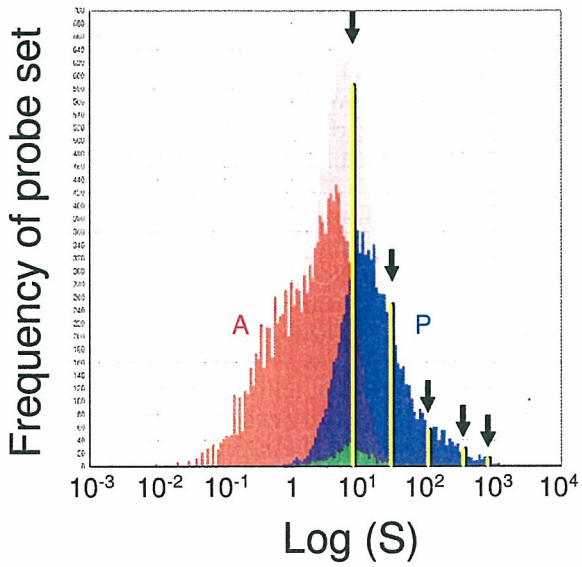

Figure 3
Positioning of GSC spike mRNAs in Affymetrix GeneChip dose-response range. A frequency histogram of the probe sets of Affymetrix GeneChip Mouse430-2 is shown. The histogram for all probe sets (gray) shows near-normal distribution. Blue columns are the "present" calls (P), red columns "absent" calls (A) and green "marginal" calls. The five yellow lines indicate the positions of the GSC spike mRNAs that are chosen to cover the "present" call range by a proper "spike factor".

total RNA to genomic DNA in a tissue type (Table 1), the spike mRNAs were calculated to correspond to 468.1, 156.0, 52.0, 17.3 and 5.8 copies per cell (diploid), respectively, for the mouse liver samples (spike factor = 0.2). The ratio of mRNAs in the cocktail is empirically chosen depending on the linear range of the measurement system and the available number of spikes. Here, we set the ratio to three to cover the "present" call probe sets of the Affymetrix GeneChip system (Figure 3).

We tested this grade-dosed spike cocktail (GSC) by Q-PCR and confirmed that the Ct values of the spike mRNAs were linearly related to the log concentrations (cf. Figure 4a), i.e. could be expressed as

$$Ct = \alpha \log C + \beta \quad \{1\}$$

The GSC was also tested by the GeneChip system and it was confirmed that the log of the spike mRNA signal intensities was linearly related to the log of their concentrations (cf. Figure 4b),

$$\log S = \gamma \log C + \delta \quad \{2\}$$

The linear relationship between the Ct values (Ct) and the log of RNA concentration (log C) was reasonable given the definition of Ct values (derived from the number of PCR cycles, i.e. doubling processes). The linear relationship between the log of GeneChip signal intensity (log S) and the log of RNA concentration (log C) was rationalized by the near-normal distribution of log S over all transcripts (cf. Figure 3).

Calculation of copy numbers of all genes/probe sets per cell

As described above, using a combination of DNA content and the spike factor of the sample, the GSC spike mRNAs become direct indicators of the copy numbers (C') per cell. When the samples were measured by Q-PCR or GeneChip analysis, the five GSC spike signals in each sample should obey function {1} for Q-PCR and function {2} for GeneChip with a good linearity. If the observed linearity was poor, a series of quality controls was performed and the measurement repeated. The coefficients of the functions were determined for each sample by the least squares method. Under the assumption that all genes/probe sets share the same signal/copy relationship, signal data for all genes/probe sets were fitted to the functions {1'} or {2'}, which are the individualized functions of {1} and {2} for each sample measurement (i).

$$Ct = \alpha i \log(C') + \beta i \quad \{1'\}$$

$$\text{Log } (S) = \gamma i \log(C') + \delta i \quad \{2'\}$$

(i = sample measurement no.)

The Q-PCR Ct values (Ct) and microarray signal values (S) of all mRNA species in the sample (i) are converted to copy numbers per cell (C') by the inverses of functions {1'} and {2'}, i.e. {3} and {4} below:

$$C' = B\text{^}((Ct-\beta i)/\alpha i) \quad \{3\}$$

for Q-PCR (Figure 4a).;

$$C' = B\text{^}((\log S-\gamma i)/\delta i) \quad \{4\}$$

for GeneChips (Figure 4b),

where B is the logarithmic base used in {1} and {2} (see Materials and Methods for details).

Real world performance of the Percellome method

The correspondence between Q-PCR and GeneChip was tested using a sample set from 2,3,7,8-tetrachlorodibenzodioxin (TCDD)-treated mice. Sixty male C57BL/6 mice

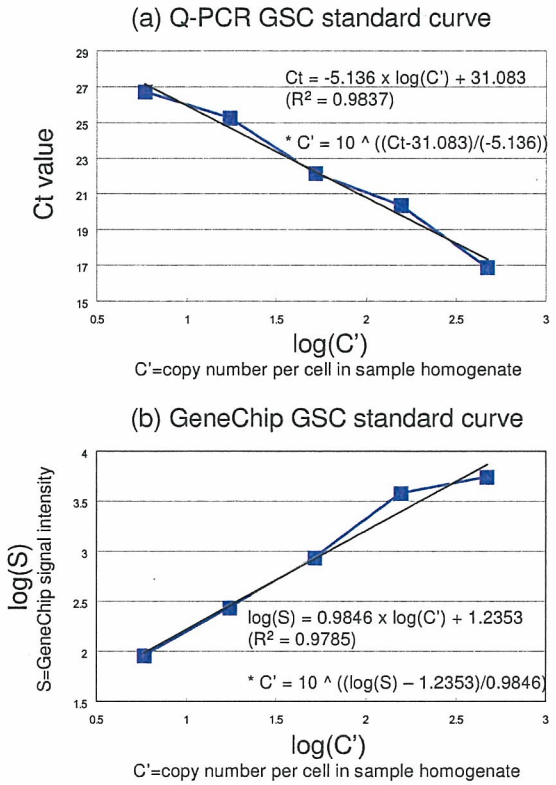

Figure 4
The dose-response linearity of the GSC spikes in Q-PCR and the Affymetrix GeneChip array system. Linear relationships are shown between (a) the Q-PCR Ct values and log of copy number (log (C')), and (b) the GeneChip log signal intensity (log(S)) and log of copy number (log (C')) of the GSC mRNAs. The regression functions were obtained by the least squares method. The inverse functions (*) were further used to generate the copy numbers of all other genes/probe sets for Percellome normalization.

were divided into 20 groups of 3 mice each. TCDD was administered once orally at doses of 0, 1, 3, 10 and 30 μg/kg, and the livers were sampled 2, 4, 8 and 24 h after administration. Nineteen primer pairs were prepared for Q-PCR and the Ct values of the liver transcriptome were measured. The same 60 liver samples were measured using the Affymetrix Mouse430-2 GeneChip [see Additional files 5 through 8 and 9 through 12]. Q-PCR and GeneChip data were normalized against cell number by functions {3} and {4}, respectively. The averages and standard deviations (sd) of each group (n = 3) were calculated and plotted as three layers of isoborograms on to 5 × 4 matrix three-dimensional graphs (Figure 5). Together with another sample set (data not shown), a total of thirty-six primer pairs were compared, and there was a correlation of up to 90% between the Q-PCR and GeneChip surfaces. It is notable that not only the average surfaces but also the +1sd and -1sd surfaces corresponded closely in shape and size. We infer that the differences resulted mainly from biological variations among the three animals in each experimental group rather than from measurement error (cf. Figure 7).

An important feature of Percellome normalization is its independence from the overall expression profile of the sample. When gene expression profiles differ among samples, Percellome normalization produces a robust transcriptome that is different from total-RNA dependent global normalization. As an example, Figure 6 shows the results of an experiment on the uterotrophic response of ovariectomized mice to estrogen treatment [12] [see Additional files 13 and 14]. The uteri of the vehicle control are atrophic because the ovaries, the source of intrinsic estrogens, are absent. The uteri of the treated groups are hypertrophic owing to estrogenic stimulus from the test compound administered. Global normalization (90 percentile) between the vehicle control group and the high-dose (1,000 mg/kg) group indicated that 4,600 of 12,000 probe sets showed 2-fold or greater increase, 470 were reduced by 0.5 or less, and 7,400 remained between these extremes. In contrast, analysis of Percellome-normalized data revealed that almost all the 12,000 probe sets showed a 2-fold or greater increase, including actin, GAPDH and other housekeeping genes. The hypertrophic tissues, consisting of cells with abundant cytoplasm, provide convincing evidence for the increases in various cellular components including housekeeping gene products.

Another important feature of Percellome normalization is the commonality of the expression scale across platforms. Batch conversion can be performed between results obtained from different platforms when the data are generated by the Percellome method. A practical strategy for such normalization is to prepare a set of samples from a target organ of interest with differences in gene expression, and measure them once by each platform. Data conversion functions with good linear dose-response relationships can be obtained individually for those genes/probe sets that are measured by both platforms (Figure 7).

Discussion

We have developed a novel method for normalizing mRNA expression values to sample cell numbers by adding external spike mRNAs to the sample in proportion to the genomic DNA concentration. For non-diploid or aneuploid samples, an average DNA content per cell should be determined beforehand for accurate adjustment. When there is significant DNA synthesis, a similar adjustment should be considered.

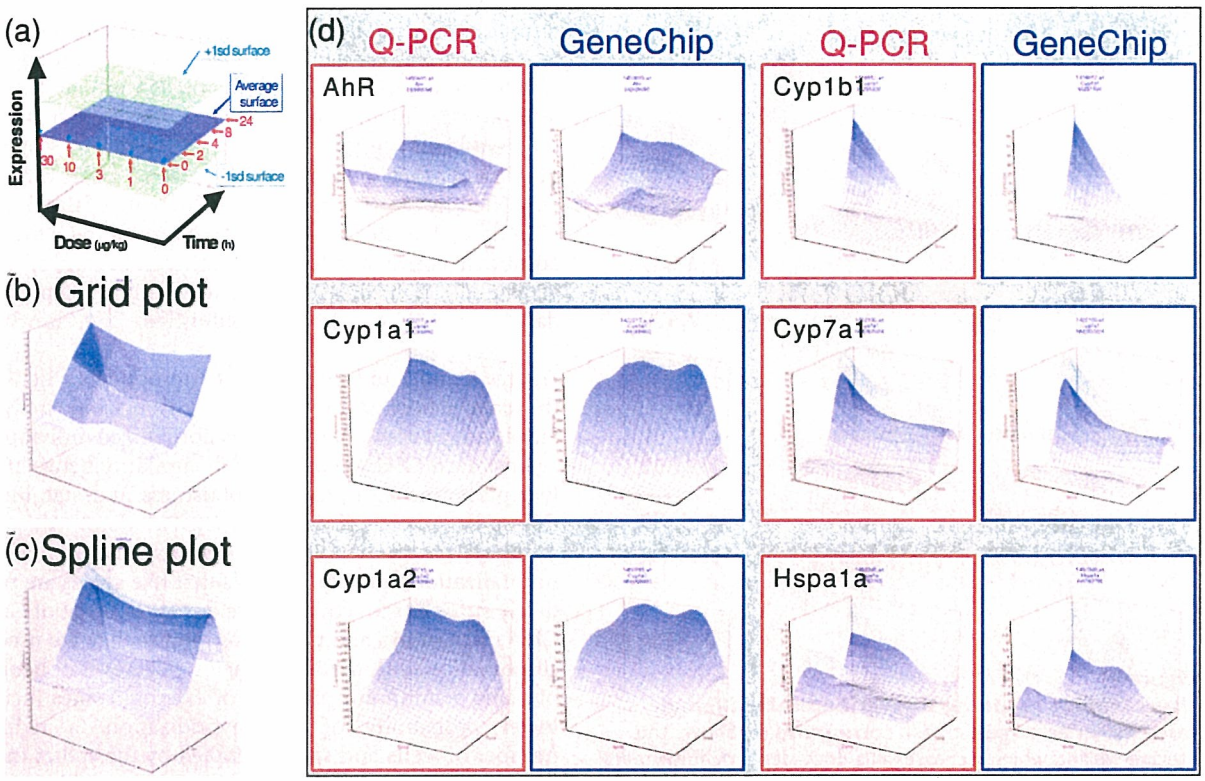

Figure 5

Correspondence between Q-PCR and GeneChip data. Sixty male C57BL/6 mice were divided into 20 groups of 3 mice each. 2,3,7,8-tetrachlorodibenzodioxin (TCDD) was administered once orally at doses of 0, 1, 3, 10 and 30μg/kg, and the liver was sampled 2, 4, 8 and 24 h after administration. The liver transcriptome was measured by the Affymetrix Mouse430-2 GeneChip. For Q-PCR, nineteen primary pairs were prepared and the Ct values of the same 60 liver samples were measured (19 genes and 5 spikes in duplicate, using a 96-well plate for 2 samples, total 30 plates). The Percellome data were plotted on to 3-dimensional graphs for average, +1sd, and – 1sd surfaces as shown in (a). The scale of expression (vertical axis) is the copy number per cell. The 0 h data (*) are copied from the 2 h/dose 0 point for better visualization of the changes after 2 h. The surfaces are demonstrated as a grid plot (b) where the grid points indicate one treatment group (n = 3), and a smoothened spline surface plot (c) for easier 3D recognition ((b), (c): Gys2 (glycogen synthase 2, 1424815_ at) showing a typical circadian pattern. (d) the smoothened plots of 6 representative genes/ probe sets generated by Q-PCR (red) and GeneChip (blue). AhR (arylhydrocarbon receptor, 1450695_at) showed imperfect correspondence. Cyp1a1 (cytochrome P450, family 1, subfamily a, polypeptide 1, 1422217_a_at) and Cyp1a2 (1450715_at) showed good correlations between Q-PCR and GeneChip except for the saturation in GeneChips above c. 400 copies per cell. Cyp1b1 (1416612_at) and Cyp7a1 (1422100_at) showed good correspondence. Hspa1a (heat shock protein 1A, 1452888_at) showed fair correspondence despite low copy numbers, near the nominal detection limit of the Affymetrix GeneChip system.

The smallest sample to which we have successfully applied the direct DNA quantification method with sufficient reproducibility is the 6.75 dpc (days post coitus) mouse embryo which consists of approximately 5,000 cells. This sample size is also approximately the lower limit for double amplification protocol to obtain sufficient amount of RNA for Affymetrix GeneChip measurement (cf. http://www.affymetrix.com/Auth/support/downloads/manuals/expression_print_manual.zip.)

High-resolution technology such as laser-capture microdissection (LCM) has become popular and the average sample size analyzed is getting smaller. An alternative method for LCM samples is to count the cell number in the course of microdissection. Although we have not yet applied Percellome method to LCM samples, we have applied the alternative method to cell culture samples to gain Percellome data. Stereological and statistical calculations should become available to correct the number of partially sectioned cells in the LCM samples. Another issue for small samples is the yield of RNA. Approximately

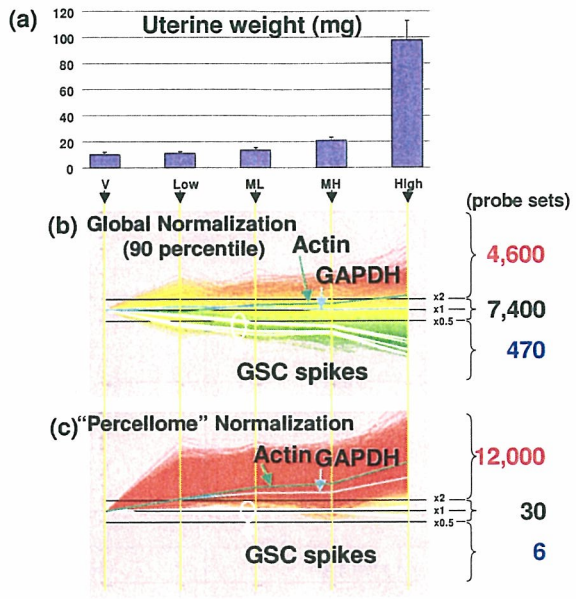

Figure 6
Uterotrophic response of ovariectomized female mice by an estrogenic test compound.(a) Shows the uterine weight, which increases in a dose-dependent manner; V, vehicle control; Low, low dose; ML, medium-low dose; MH, medium-high dose; High, high dose group. (b) Shows the line display of uterine gene expression (Affymetrix MG-U74v2 A GeneChips) normalized by global normalization (90 percentile), and (c) by the Percellome normalization. Averages of three samples per group were visualized (by K. A.). The five white lines are the GSC mRNAs. The green and blue lines are actin (AFFX-b-ActinMur/M12481_3_at) and GAPDH (glyceraldehyde-3-phosphate dehydrogenase, AFFX-GapdhMur/M32599_3_at), respectively. By global normalization, 7,400 probe sets remained unchanged and 4,600 probe sets increased more than two-fold in the H group compared to the V group, whereas almost all probe sets measured had increased. It is noted that housekeeping genes such as actin and GAPDH are significantly induced on a per cell basis.

30 ng of total RNA is retrieved from a single 6.75 dpc mouse embryo. This amount is sufficient for a double amplification protocol (DA) to prepare enough RNA for an Affymetrix GeneChip measurement. An inherent problem with the DA data is that the gene expression profile differs from that of the default single amplification protocol (SA). Consequently the DA percellome data differ from that of SA as if they were produced by a different platform. To bridge the difference, we applied the procedure that was used for data conversion between Q-PCR and GeneChip (cf. Figure 7). A set of spiked-in standard samples including the LBM sample set (of sufficient concentration) were measured by the SA protocol and diluted versions to the limit measured by the DA protocol. These data provided us with information about whether DA was successful as a whole (by comparing 5' signal to 3' signals of selected probe sets) and which probe sets were properly amplified by DA (by checking the linearity of the diluted LBM data). For those probe sets that proved to be linearly amplified, conversion functions between DA and SA were generated. These details, along with embryo expression data will be published elsewhere.

Figures 5 and 7 indicate a close correspondence between the data generated by Q-PCR and GeneChip analyses. Since each of the 60 samples was normalized individually against each GSC signal, the high similarity between the two platforms indicates the robustness and stability of this spike system (cf. Figure 7, Cyp7a1 data). Although more spikes could potentially increase the accuracy of normalization, our experience is that five spikes are practically sufficient for covering the detection range of GeneChip microarrays and Q-PCR, as long as they are used in combination with the "spike factor". The overall benefits of using a minimum number of external spikes include lower probability of cross-hybridization, a reduced number of wells and spots occupied by the spikes in the Q-PCR plates and small scale microarrays, and less effort in preparation, QC and supply.

The Percellome data can be truly absolute when all mRNA measurements including GSC spikes are strictly proportional to the original copy numbers in the sample homogenate. As noted earlier, this condition is not guaranteed by any platform despite linearity of response. Therefore, the Percellome-normalized values have some biases for each primer pair/probe set, depending on the steepness of the dose-response curves. An advantage of Percellome normalization is that, as long as such biases are consistently reproduced within a platform, the data can be compared directly among samples/studies on a common scale. Consequently, when a true value is obtained by any other measure, all the data obtained in the past can be simultaneously batch-converted to the true values.

This batch-conversion strategy can be extended to data conversion between different versions and different platforms, as long as the data are generated in copy numbers "per cell". We have shown an example between Affymetrix GeneChip and Q-PCR for limited numbers of probe sets (cf. Figure 7). Custom microarrays that accept our GSC for Percellome normalization are in preparation by Agilent Technologies (single color) and GE Healthcare (CodeLink Bioarray).

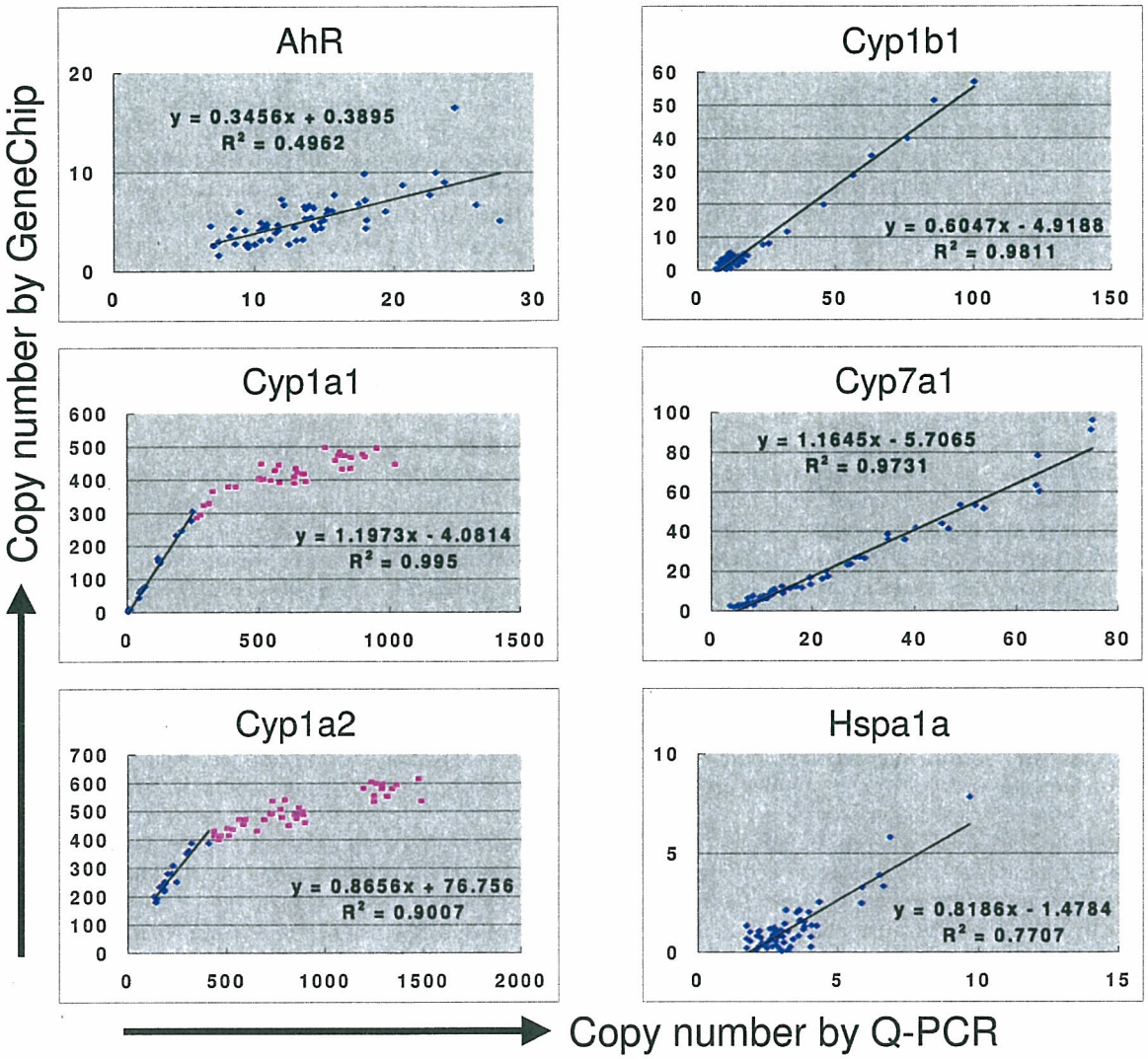

Figure 7
Conversion functions between Q-PCR and GeneChip. The data shown in Figure 5 as 3D surfaces are shown as a scatter plot (60 plots). The regression function can be used to convert Q-PCR to GeneChip and vice versa, with a level of certainty indicated by coefficient of correlation. It is noted that Cyp1a1 and Cyp1a2 became saturated above about 400 copies per cell in GeneChip system (indicated in pink plots). Cyp7a1 showed high linearity, indicating that the variation shown by the split +1sd and -1sd surfaces in Figure 5 reflected biological (animal) variation, not measurement errors.

Another important contribution of Percellome analysis is in the area of archived data in private and public domains. Firstly, Percellome data are the result of a simple linear transformation of the raw microarray data; preserving the distribution and order of the probe set data. Therefore, parametric or non-parametric methods should be able to align the data distribution and generate estimates of mRNA copy number of the non-spiked archival samples. Any archival samples that are re-measurable by Percellome method will greatly increase the accuracy of estimation. Secondly, percellome can provide appropriate bridging information between old and new versions of Affymetrix GeneChips, such as human HU-95 and HU-133, murine MU-74v2 and MOE430 series. This should also facilitate comparisons between newly generated and archived data.